Geomorphic and structural variations along the Doruneh Fault System (central Iran)

Yassaman Farbod, Olivier Bellier, Esmaeil Shabanian, Mohammad Reza Abbassi

Geomorphic and structural variations along the Doruneh Fault System (central Iran)

Yassaman Farbod,[1,2] Olivier Bellier,[1] Esmaeil Shabanian,[1] and Mohammad Reza Abbassi[2]

Received 11 February 2011; revised 15 September 2011; accepted 14 October 2011; published 21 December 2011.

[1] This paper focuses on the analysis of geomorphic, structural, and behavioral characteristics along the Doruneh Fault System (DFS), east of longitude 56°45′E. Detailed geomorphic and structural analyses of different scale satellite images and digital topographic data, accompanied with field surveys allowed us to establish a fault segmentation model in which three discrete fault zones have been recognized: (1) the western fault zone (WFZ) characterized by reverse left-lateral mechanism with left-handed step-over geometry, (2) the central fault zone (CFZ) which is pure left-lateral strike-slip and comprises nearly parallel faults, and (3) the eastern fault zone (EFZ) that is a trailing imbricate fan fault-termination characterized by reverse faulting and fault-related folding. Each fault zone shows discrete geometry and kinematics implying that deformation is not uniformly accommodated along the DFS. We propose a new kinematic model to explain how the DFS accommodate the Arabia-Eurasia convergence normal to the overall fault orientation. According to this model, the DFS takes up the northward motion between central Iran–Lut block relative to Eurasia by a complex kinematics varying from pure reverse to pure left-lateral strike-slip faulting. The kinematics of the WFZ and EFZ corresponds to the direction of the NE-trending regional compression. While, the partitioning of slip into strike-slip and reverse component of faulting on parallel faults (strain partitioning) allows the CFZ to remain pure left-lateral strike-slip. Such a model propose a way to explain how large strike-slip faults such as the DFS accommodate tectonic block motions perpendicular to strike of the faults.

Citation: Farbod, Y., O. Bellier, E. Shabanian, and M. R. Abbassi (2011), Geomorphic and structural variations along the Doruneh Fault System (central Iran), *Tectonics*, *30*, TC6014, doi:10.1029/2011TC002889.

1. Introduction

[2] As common features in intracontinental deformation domains, long straight strike-slip fault systems such as the Doruneh, Neh, and Nayband faults affect the seismically active Iranian plateau (Figure 1). The seismogenic behavior of a few individual faults have locally been characterized thank to paleoseismologic studies [e.g., *Hessami et al.*, 2003; *Ritz et al.*, 2006; *Nazari et al.*, 2009; *Solaymani*, 2009], or thank to a rich, but local, historical and archeological record spanned several thousand years [e.g., *Ambraseys and Melville*, 1982; *Berberian and Yeats*, 1999, 2001], as well as occurrences of large ($M \geq 6$) instrumental earthquakes. However, the historical records of earthquakes are biased toward regions close to trade routes, and are not complete everywhere around the country. Thus, the seismogenic behavior of other large faults remains unknown due to the lack of instrumental and/or historical earthquake records along and in the vicinity of those faults.

[3] In Central Iran, the geologically active Doruneh Fault System (Figure 1) has not sustained historical earthquakes of magnitudes $M \geq 6$, raising the possibility that it could produce earthquakes of large ($M \geq 8$) magnitudes [*Berberian and Yeats*, 1999] resulting in a high seismic hazard. The explanations for such a hypothesis could be (1) a long recurrence interval of several thousand of years [*Berberian and Yeats*, 1999; *Fattahi et al.*, 2007] during which the large faults are accumulating strain and no energy release occurred by seismic or aseismic displacements, and (2) the fact that the Doruneh Fault has been far from historical trade routes that may caused a non-complete records of large historical earthquakes, which probably occurred on and around the fault.

[4] Nevertheless, there are general consensuses that fault zones, particularly long ones, do not rupture along their entire length during a single earthquake [*King and Nabelek*, 1985; *Barka and Kadinsky-Cade*, 1988; *Knuepfer*, 1989; *Schwartz and Sibson*, 1989; *DePolo et al.*, 1991; *McCalpin*, 1996; *Stewart and Taylor*, 1996; *Barka et al.*, 2002; *Kondo et al.*, 2005; *Ikeda et al.*, 2009]. Actually, such apparently continuous long fault systems could be divided into discrete

[1] Aix-Marseille Université, CEREGE, CNRS UMR 6635, Aix en Provence, France.
[2] International Institute of Earthquake Engineering and Seismology, Tehran, Iran.

0278-7407/11/2011TC002889

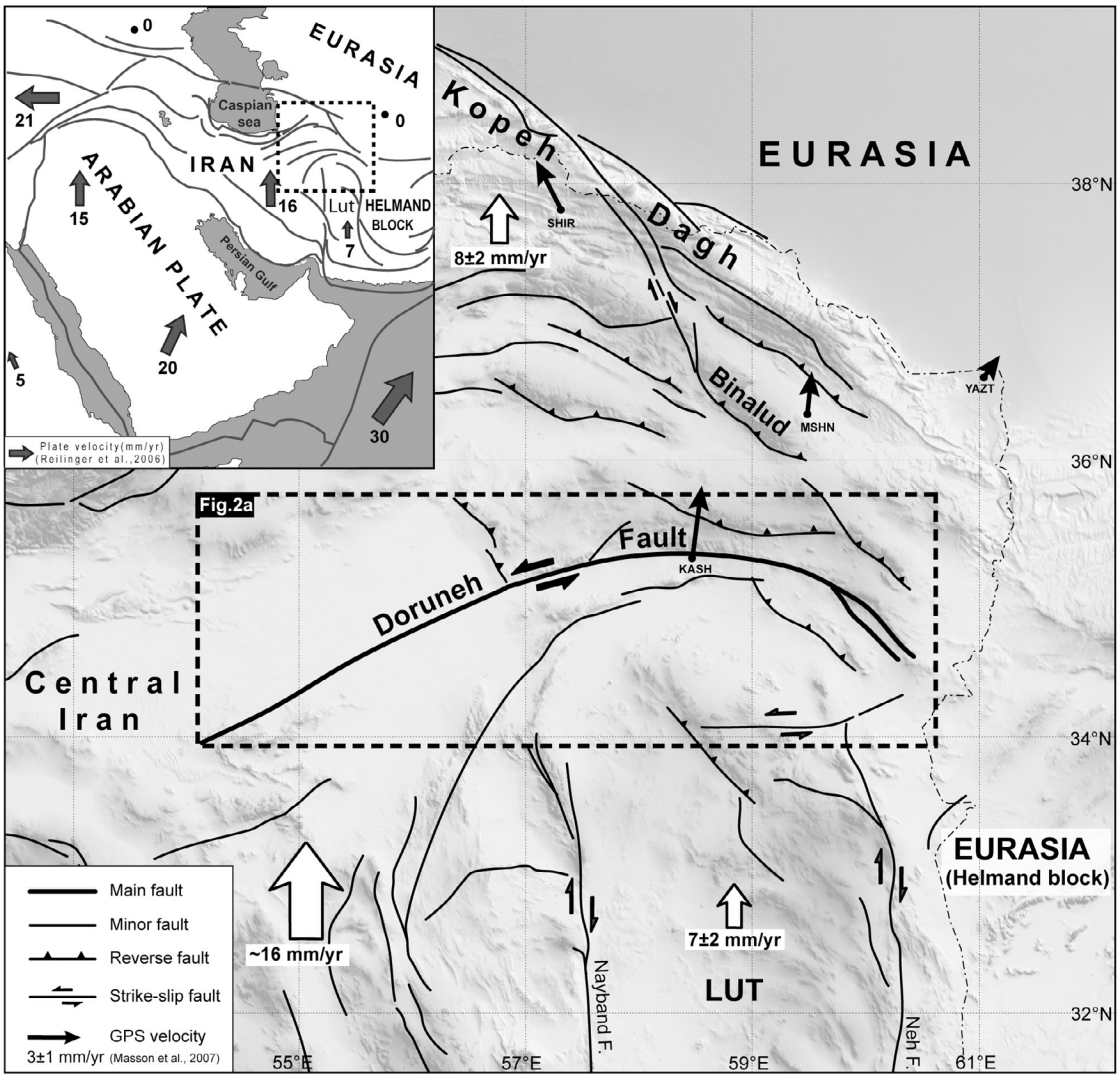

Figure 1. GTOPO30 topographic image of central and northeastern Iran showing the location of the Doruneh Fault together with principal deformation domains and structural units mentioned in the text. Black arrows are GPS horizontal velocities (mm/yr) in a Eurasia-fixed reference frame (YAZT station [*Masson et al.*, 2007]). White arrows, south of the Doruneh Fault are geodetic-derived tectonic motions after *Reilinger et al.* [2006], while the white arrow in the Kopeh Dagh is the geologic rate of the western Kopeh Dagh–Eurasia northward motion [*Shabanian et al.*, 2009a]. The box in the upper left inset shows the location in the Arabia–Eurasia collision zone. Grey arrows and associated numbers represent Arabia–Eurasia plate velocities (mm/yr) after *Reilinger et al.* [2006].

fault zones or segments, at a variety of scales, that have different geometries, faulting histories and seismicity [e.g., *Schwartz and Coppersmith*, 1984; *Bruhn et al.*, 1987; *Knuepfer*, 1989; *DePolo et al.*, 1991; *Stewart and Taylor*, 1996]. The first stage to understand the seismogenic behavior of large strike-slip fault systems is the identification of distinct fault zones and/or fault segments together with their persistent boundaries, i.e., to establish a fault segmentation model.

[5] Various types of segmentation models, based on seismological data and surface geological features, have been proposed for seismic hazard assessment within active strike-slip fault systems [e.g., *DePolo et al.*, 1991; *Lees and Nicholson*, 1993; *McCalpin*, 1996; *Nishigami*, 2000; *Lettis et al.*, 2002; *Kondo et al.*, 2005]. In ideal fault segmentations, the aim is to identify the part of a fault zone that will rupture as an independent segment and, within the segment, identify the nucleation point of the earthquake. Nevertheless, segments may present a long fault with a length of tens to hundreds of kilometers, or they may represent an individual fault rupture only a few kilometers in length. As the term "segment" was not explicitly defined, we use the term segmentation for the division of a large fault system into fault zones with distinct geomorphic, structural, and behavioral characteristics.

[6] The twofold aim of this paper is (1) to provide evidence of geomorphic, structural, and fault behavioral variations [cf. *Knuepfer*, 1989] using which a fault segmentation model for the DFS, at the scale of fault zones, can be established, and (2) to address the way that active

deformation is accommodated along the fault system. These two objectives lead to better understand the seismic potential of different sectors of the DFS, and the contribution of the entire fault system in the accommodation of ongoing deformation in NE Iran. The results of this study may be useful to explain how large strike-slip faults such as the DFS take up overall tectonic block motions perpendicular to their strike.

2. Tectonic and Geological Setting

[7] The Iranian plateau is deformed as a collisional domain between the converging Arabian and Eurasian plates. The convergence rate increases eastward reaching 26 ± 2 mm/yr at a longitude of 59°E, south of the Persian Gulf [*Sella et al.*, 2002; *McClusky et al.*, 2003; *Vernant et al.*, 2004; *Reilinger et al.*, 2006]. This plate motion results in right-lateral shear between central Iran and Eurasia at a rate of ∼16 mm/yr [e.g., *Vernant et al.*, 2004; *Regard et al.*, 2005] involving major N-trending strike-slip fault systems [*Tirrul et al.*, 1983; *Regard et al.*, 2004; *Walker and Jackson*, 2004; *Meyer and Le Dortz*, 2007] (Figure 1). Further north, in northeast Iran, the available geodetic data [*Vernant et al.*, 2004; *Masson et al.*, 2007; *Tavakoli*, 2007] indicate a northward displacement rate ranging from 4 to 9 mm/yr for the western Kopeh Dagh with respect to Eurasia. The geological rate of this northward motion is estimated at 8 ± 2 mm/yr [*Shabanian et al.*, 2009a]. At a latitude of ∼35°N, the area between northern deformation domains (i.e., the Alborz, Kopeh Dagh and Binalud mountain ranges) and the southern N-S fault systems is separated by the "Doruneh Fault" [e.g., *Tchalenko et al.*, 1973; *Mohajer-Ashjai*, 1975], which preclude their direct structural connections.

[8] The term "Doruneh Fault" has been used for the longest strike-slip fault in the Iranian plateau [*Wellman*, 1966], which runs east-west over a ∼600 km length between longitudes of 54°E and 60°30′E (Figure 1). The general trace of the Doruneh Fault, which was mapped on regional scale geological maps [*Stocklin and Nabavi*, 1973; *Eftekhar-Nezhad et al.*, 1976; *Huber*, 1977], indicates a bow-shape northward convex structure comprising two distinct parts, with different orientations. The preliminary division of the Doruneh Fault into two sectors [*Tchalenko et al.*, 1973; *Mohajer-Ashjai*, 1975] was based on the change in the orientation of the fault trace from NE to E at the longitude of Doruneh village (Figure 2a). However, new structural and geomorphic mapping complemented by preexisting data (geological maps and their associated cross sections) indicate that the structural boundary between the western and eastern parts does not closely coincide with the location of Doruneh village. But, further west, at a longitude of 56°45′E, there is evidence of drastic changes in geologic, structural and geomorphic expression of the fault (Figure 2a), where there is a ∼40-km-long structural gap along which Quaternary deposits have not been affected by the fault activity. From there, the western part (i.e., Great Kavir Fault) runs southwest for ∼275 km through the Great Kavir desert (Dasht-e Kavir), and left-laterally cuts the dome and basin structures of the folded Tertiary rocks. Along its entire length, the western part passes within the upper Miocene sandstones and marls (Upper Red Formation) without significant change in the topography on either sides of the fault. The surface geometry of the fault is characterized by left-handed arrangements of multiple fault segments. Releasing offsets between stepover fault segments occupied by pull-apart basins of different scales which are filled by Quaternary deposits (Figure 2b).

[9] The eastern part, which we term the Doruneh Fault System (DFS), is a ∼360-km-long E-trending fault system separating the pre-Oligocene paleoreliefs to the north from the folded Neogene piedmont armored by Quaternary deposits to the south (Figure 2c). In other words, the DFS forms a geological and topographic boundary between the northern mountain ranges, with an average elevation of ∼2500 m, and the southern Quaternary plain with a mean elevation of ∼1200 m. Along the DFS, the moderately folded Miocene rocks, crop out in the southern side, contrast intensely folded and faulted Paleozoic to Eocene sedimentary rocks of the northern side, which have been intruded by Upper Cretaceous to upper Eocene volcanic rocks. The lack of Neogene deposits on the northern part of the DFS suggests that vertical faulting during Oligocene and Miocene along the DFS controlled the northern margin of the sedimentary basin. Such a geological characteristic sets apart the DFS from the Great Kavir Fault, which clearly cuts and laterally offset the post-Miocene geological structures through the Dasht-e Kavir lowlands [e.g., *Walker and Jackson*, 2004], without any evidence of vertical faulting. That means the Oligo-Miocene Dasht-e Kavir sedimentary basin spreads either side of the fault, and was not controlled by vertical faulting along the Great Kavir Fault. Hereafter, we present geomorphic and structural investigations leading us to characterize the pattern and kinematics of active faulting along the DFS, and subsequently, to establish a fault segmentation model, at the scale of fault zones.

3. The Doruneh Fault System (DFS)

[10] The DFS is an arcuate structural assemblage, with a complex history of tectonic evolution along which there is clear evidence of at least two distinct periods of faulting during the Cenozoic: (1) an initial vertical faulting that controlled the northern margin of the subsiding Neogene sedimentary basin located on the southern side of the fault, and (2) Quaternary strike-slip movements affecting post-Miocene geological structures and geomorphic landforms. There is a striking contrast between Cenozoic rocks on opposite sides of the DFS. The northern domain is characterized by Paleozoic to Eocene rocks while in the southern part, Neogene and Quaternary deposits are crop out (Figure 2c). The lack of Miocene sedimentation on the northern side indicates direct structural control of the DFS due to its vertical movements on the geological evolution of the bounding sedimentary basin. The same sedimentary and volcano-clastic rock series of Jurassic-Cretaceous and Eocene on either sides of the fault [e.g., *Huber*, 1977] suggest the post-Eocene onset of vertical movements along the DFS. The total vertical slip of the earlier movements along the fault system is unclear; no rocks of post Eocene series have been matched across the fault system. On the southern side, the Eocene rocks are overlain by more than 2000 m of Neogene-Quaternary deposits [*Huber*, 1977; *Alavi-Naini et al.*, 1992] that have no counterpart. On the other hand, the present-day average topographic level of the

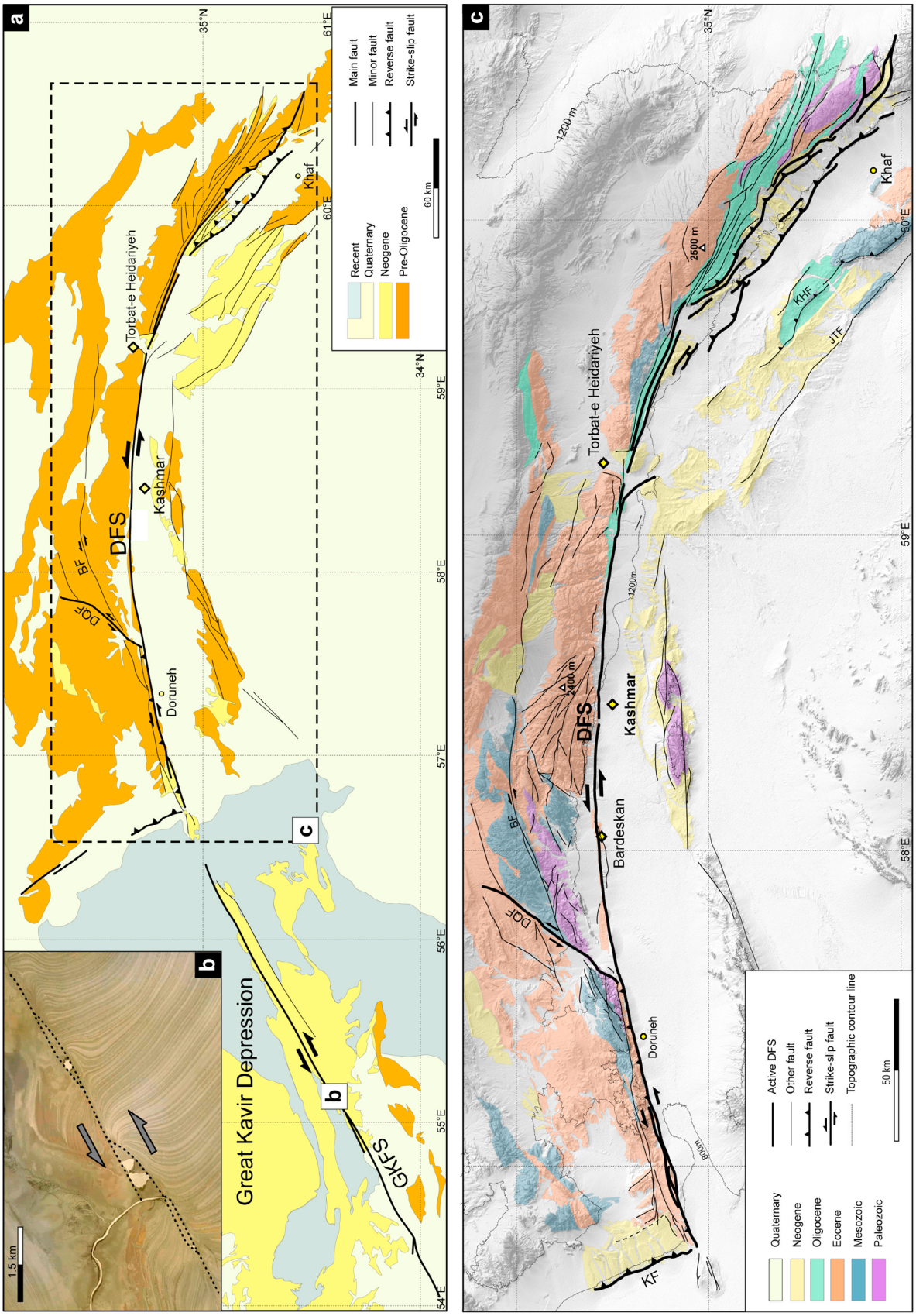
a
b
c
DFS
BF
DOF
GKFS
KF
KHF
JTF
Torbat-e Heidariyeh
Kashmar
Doruneh
Khaf
Bardeskan
Great Kavir Depression
Main fault
Minor fault
Reverse fault
Strike-slip fault
Recent
Quaternary
Neogene
Pre-Oligocene
60 km
1.5 km
1200 m
2500 m
2400 m
1200m
800m
50 km
Active DFS
Other fault
Reverse fault
Strike-slip fault
Topographic contour line
Quaternary
Neogene
Oligocene
Eocene
Mesozoic
Paleozoic
35°N
34°N
54°E
55°E
56°E
57°E
58°E
59°E
60°E
61°E

Figure 2

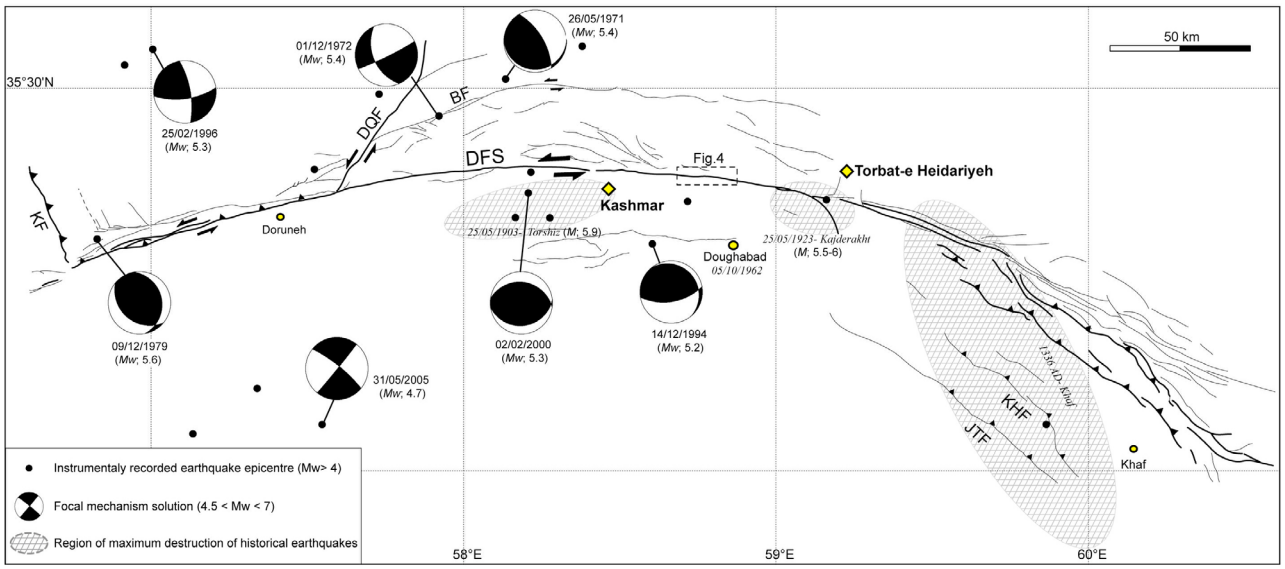

Figure 3. Historical and instrumental seismicity of the DFS and surrounding areas. Focal mechanisms are mainly taken from the Harvard catalog (http://www.globalcmt.org/CMTsearch.html) and *Jackson and McKenzie* [1984]. Epicenters are from the ISC EHB Bulletin (International Seismic Centre, Thatcham, United Kingdom, 2009, http://www.isc.ac.uk). The regions of maximum destruction are based on *Ambraseys and Melville* [1982].

Eocene paleoreliefs north side of the fault is about 1200 m above the average topographic level of the southern part. If the earlier movement was vertical, a minimum displacement of ~3200 m is necessary to achieve the present-day configuration, though the general history of movement on the fault system remains unknown. Nevertheless, conspicuous geomorphic offsets recorded by alluvial fans and streams indicate a prominent left-lateral strike-slip kinematics for the late Quaternary activity of the DFS (section 4.2).

[11] Along the DFS and in nearby areas, the historical [*Ambraseys and Melville*, 1982] and instrumental [e.g., *Tchalenko*, 1973; *Tchalenko et al.*, 1973; *Jackson and McKenzie*, 1984; *Fattahi et al.*, 2007] records of ~700 years seismicity indicate moderate seismicity despite clear late Pleistocene and Holocene activity of the fault system. The earliest recorded historical event is the earthquake of 1336 AD, which destroyed a wide area of 110 × 40 km^2, extended between Torbat-e Heidariyeh and Khaf (Figure 3) causing about thirty thousand deaths [*Ambraseys and Melville*, 1982]. The region of the maximum destruction is located along the NW-trending Jangal thrust fault that runs parallel, and to the west of the eastern termination of the DFS. Another historical earthquake occurred in 1619, and damaged several villages south of Torbat-e Heidariyeh and also totally destroyed the village of Dugh-Abad (Figure 3). It was suggested that the earthquake was a large magnitude event causing a lot of damage and almost 800 deaths during the day [*Ambraseys and Melville*, 1982]. The two ~45 km-apart damaged zones of the 1903 (Turshiz M = 5.9 [*Ambraseys and Melville*, 1982]) and 1923 (Kajderakht M = 5.5–6 [*Tchalenko*, 1973]) earthquakes are located just south of and along the main trace of the DFS, respectively (Figure 3). During the field work, ~30 km west of the damaged area of 1923 earthquake (near Forsheh village) we observed evidence of a coseismic left-lateral surface rupture zone that is composed of overlapping fault segments (Figure 4). The releasing structural offsets between adjusting segments are occupied by pull-apart basins, while restraining stepovers are the place of en echelon pressure ridges. The rupture zone and its associated geomorphic landforms have been developed in the lower (youngest) alluvial fan surface above the current streambed (Figure 4). Clear deflections of streams around the ~2-m-high pressure ridges together with a lack of incision at the top of ridges confirm the coseismic nature of the landforms. Assuming that a single event produced such a rupture zone, a total rupture length of ~11.5 km (Figure 4) suggests a magnitude of ~6.3 for that seismic event. However, given the relatively large distance (~30 km) between the rupture zone and the location of damage zones of both 1903 and 1923 earthquakes (Figure 3), the event or events that produced these features remain unknown.

Figure 2. (a) Simplified geological map of the region affected by the Doruneh (DFS) and Great Kavir (GKFS) fault systems. Geological units are from *Huber* [1977]. (b) Examples of pull-apart basins formed between releasing left-handed stepovers along the GKFS that cuts through dome and basin structures in the Miocene deposits (Quickbird image from GoogleEarth). (c) Detailed geological map of the Doruneh Fault System (modified after *Eftekhar-Nezhad et al.* [1976] and *Alavi-Naini et al.* [1992]) superposed on shaded relief image of the area (SRTM digital topographic data). Fault traces in Figures 2a and 2c are based on geomorphic and structural analyses of SPOT5 and LANDSAT ETM+ (this study). Abbreviations are: BF, Bijvard Fault; DQF, Dahan-Qaleh Fault; KF, Kharturan Fault; KHF, Khaf Fault; JTF, Jangal Thrust Fault.

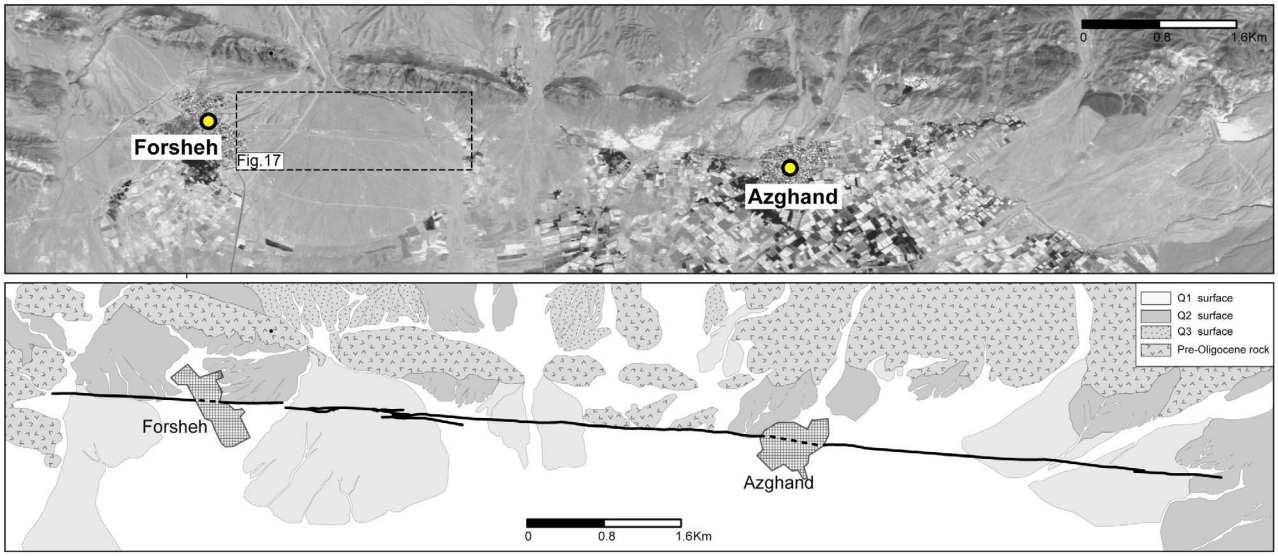

Figure 4. Simplified morphotectonic map of the rupture zone along the CFZ, in the Forsheh area. See text for more information.

[12] Focal mechanism solutions of instrumental earthquakes ($M \geq 4.5$) are shown in Figure 3, and are listed in Table 1. No instrumental, and consequently, earthquake focal mechanism can directly be assigned to the Doruneh Fault. Nearly 60 per cent of the solutions in the vicinity of the fault (a distance of ~30 km from the fault line) show prominently thrust faulting on fault planes in various directions. The focal mechanism of 1971 earthquake indicates left-lateral faulting on a southward gently dipping (26°S) nodal plane or dextral faulting on a nearly vertical NW-SE nodal plane, both inconsistent with geometry of the Doruneh Fault. Two of other three focal mechanism solutions of 1972, 1994 and 2000 earthquakes (i.e., 1994 and 2000 earthquakes) located near the Doruneh Fault show nearly pure thrusting on E-W fault planes. The explanation for reverse faulting on E-W planes indicated by these focal mechanism solutions remains unclear; *Fattahi et al.* [2007] attributed the 2000 event to undefined north-dipping east-west thrusts. In section 6.1, we discuss possible relationships between these earthquakes and the Doruneh Fault in the light of geomorphic and structural data. The focal mechanism solution of 1972 earthquake indicates strike-slip faulting along a NE-SW plane. Considering both the location and fault geometry of this solution, it is more likely that the 1972 earthquake to be related to the Bijvard Fault (Figure 3).

[13] The epicenter of 9 December 1979 earthquake is located close to the DFS, ~50 km west of Doruneh village (Figure 3). Harvard CMT solution of this event represents nearly pure reverse faulting along N-trending nodal planes (Figure 3). An alternative strike-slip solution has been proposed by *Jackson and McKenzie* [1984] showing left-lateral faulting on an ENE-trending nodal plane. This solution has been preferred by *Jackson and McKenzie* [1984] because it was more consistent with the general orientation of the western part of the DFS. However, a detailed mapping of the western termination of the DFS (section 4.1.1) led to evaluate the geological reliability of these two solutions indicating that the reverse mechanism (Harvard CMT solution) is more consistent with both the structural pattern and geometry of the fault system.

[14] In summary, both the instrumental and historical records of earthquakes indicate that the region affected by the DFS experienced a moderate seismicity when compared to nearby seismic regions such as the Kopeh Dagh [*Tchalenko and Berberian*, 1975; *Berberian and Yeats*, 1999, 2001; *Hollingsworth et al.*, 2006; *Shabanian et al.*,

Table 1. Epicenters and Source Parameters of Earthquakes Affecting the Nearby Region of the Doruneh Fault System[a]

ID	Date (dd.mm.yyyy)	Longitude (°E)	Latitude (°N)	Mw	Plane 1			Plane 2			Depth (km)
					Azimuth	Dip	Rake	Azimuth	Dip	Rake	
1	26.05.1971	58.135	35.525	5.4	88	26	31	329	76	112	26
2	01.12.1972	57.922	35.428	5.4	156	65	−176	64	87	−25	33
3	09.12.1979	56.827	35.107	5.6	350	44	121	129	53	63	15
4	14.12.1994	58.604	35.094	5.2	319	32	144	80	72	63	33
5	25.02.1996	56.948	35.72	5.4	82	77	10	350	80	166	33
5	02.02.2000	58.207	35.227	5.3	83	43	79	278	48	100	26
6	31.05.2005	57.626	34.306	4.9	309	84	−1	39	89	−174	25

[a]Focal mechanisms of the two first events are from *Jackson and McKenzie* [1984], and events 3 to 6 are taken from the Harvard catalog (http://www.globalcmt.org/CMTsearch.html). Epicenters are from ISC, EHB Bulletin (http://www.isc.ac.uk).

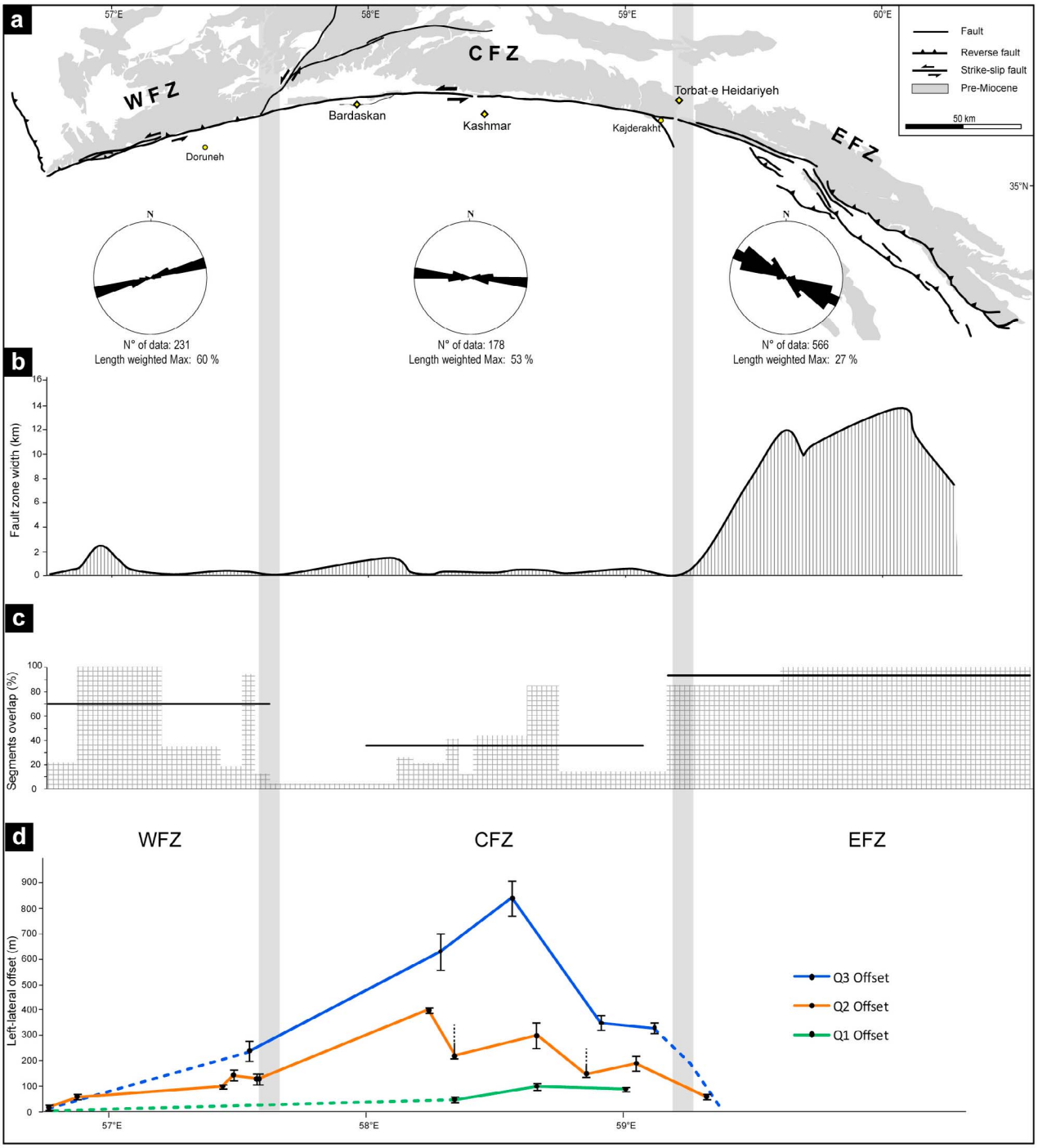

Figure 5. (a) General fault map of the DFS comprising three discrete fault zones. Rose diagrams represent the predominant orientation of the fault zones deduced from the statistic analysis of individual fault segments, which have been mapped on SPOT5 satellite images. (b) Along-strike variations in the wideness of the DFS. The initiation point of the diagram is the western termination of the WFZ. (c) Spatial variations in the geometric arrangement of fault segments within the DFS are illustrated by plotting the straight length of individual fault segments versus the total overlap length of each segment that is covered by other nearby faults. Thick lines indicate the average value of the segment overlap in each fault zone. (d) along-strike variations in cumulative left-lateral offsets of the DFS. Uncertainty of the offset measurement is shown by error bars.

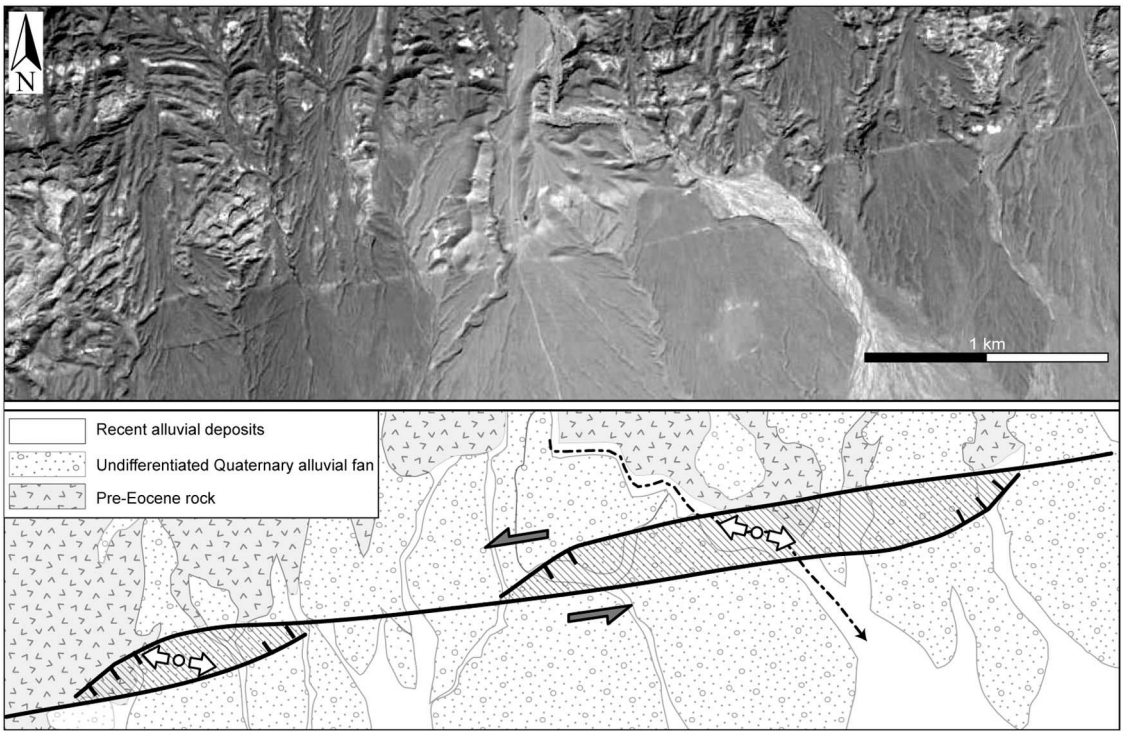

Figure 6. SPOT5 image centered on two pull-apart basins (hatched areas) formed in releasing offsets between overlapping segments of the WFZ; see Figure 7 for the location.

2009b] and northern margin of the Lut block [*Berberian and Yeats*, 1999; *Walker et al.*, 2003, 2004, and references therein].

4. Fault Segmentation

[15] At the regional scale, the DFS seems a continuous curved structure that runs northeast from a longitude of 56°45′E for about 125 km to ~12 km to the northeast of Bardeskan town (Figure 5), where it turns ~15° eastward and continues for about 75 km. The fault trace takes another bend (~20° clockwise) at a longitude of 59°15′E and continues for ~160 km toward the southeast. Given that such a large scale change in the surface geometry of a fault may result in variations in both the slip rate and kinematics of the fault, each portion of the ~360-km-long DFS can represent a distinct fault zone with the characteristic geometry, structure and fault behavior. In this section we present structural and geomorphic analyses conducted along the DFS in order to establish, at the scale of fault zones, a fault segmentation model. In this way, we take heed of (1) the geometry and kinematics of discrete fault zones, (2) spatial variations in the amount and nature of Quaternary geomorphic offsets (3) the size and geometry of structural discontinuities along the fault system, and (4) changes in complexity of fault trace, in the sense of fault slip, and in the die-out of fault trace beyond which no active faulting is mapped [cf. *Knuepfer*, 1989].

4.1. Variations in the Structural and Geometric Characteristics of the DFS

[16] According to our detailed structural mapping of the entire fault system, the DFS is constituted by multiple individual fault segments. A statistical analysis of the orientation of fault traces longer than 5 km clearly illustrates three structural fault portions with different orientations (Figure 5a): (1) the western part between 56°45′ and 57°37′ that is principally oriented in the N75 ± 5°E direction, (2) the central part that continues eastward (N95 ± 5°) up to a longitude of 59°15′, and (3) the N130 ± 10°E-trending eastern part. These variations in the fault strike are followed by changes in the width of the fault system (Figure 5b) such that the DFS becomes wider at both the eastern and western terminations. The western part reaches ~2.5 km in width joining the relatively narrow ≤0.4-km-wide linear central part (Figure 5b). Interestingly, the maximum width of the western part is observed at its structural terminations where the fault movements is transmitted to transpressional relay zones forming complex reverse pop-up structures. The linear pattern of the central part contrasts with the ~14-km-wide eastern part, which is composed of numerous imbricate reverse fault segments (Figure 5b).

[17] The presence of three distinct fault zones is also confirmed by examining changes in the geometric arrangement of fault segments constituting each fault zone. For instance, along the western part, fault segments show mostly a left-stepping arrangement, whereas to the east a parallel fault arrangement is dominated. The central part of the DFS is more complex than the two other parts such that both parallel and en-echelon arrangements are found. Such a variation was illustrated by plotting the straight length of individual fault segments versus the total overlap length of each segment that is covered by other nearby faults (Figure 5c). Within the western part, almost ~70 per cent of the total length of each fault segment is overlapped by one or more adjacent segments. In the eastern part, fault segments are

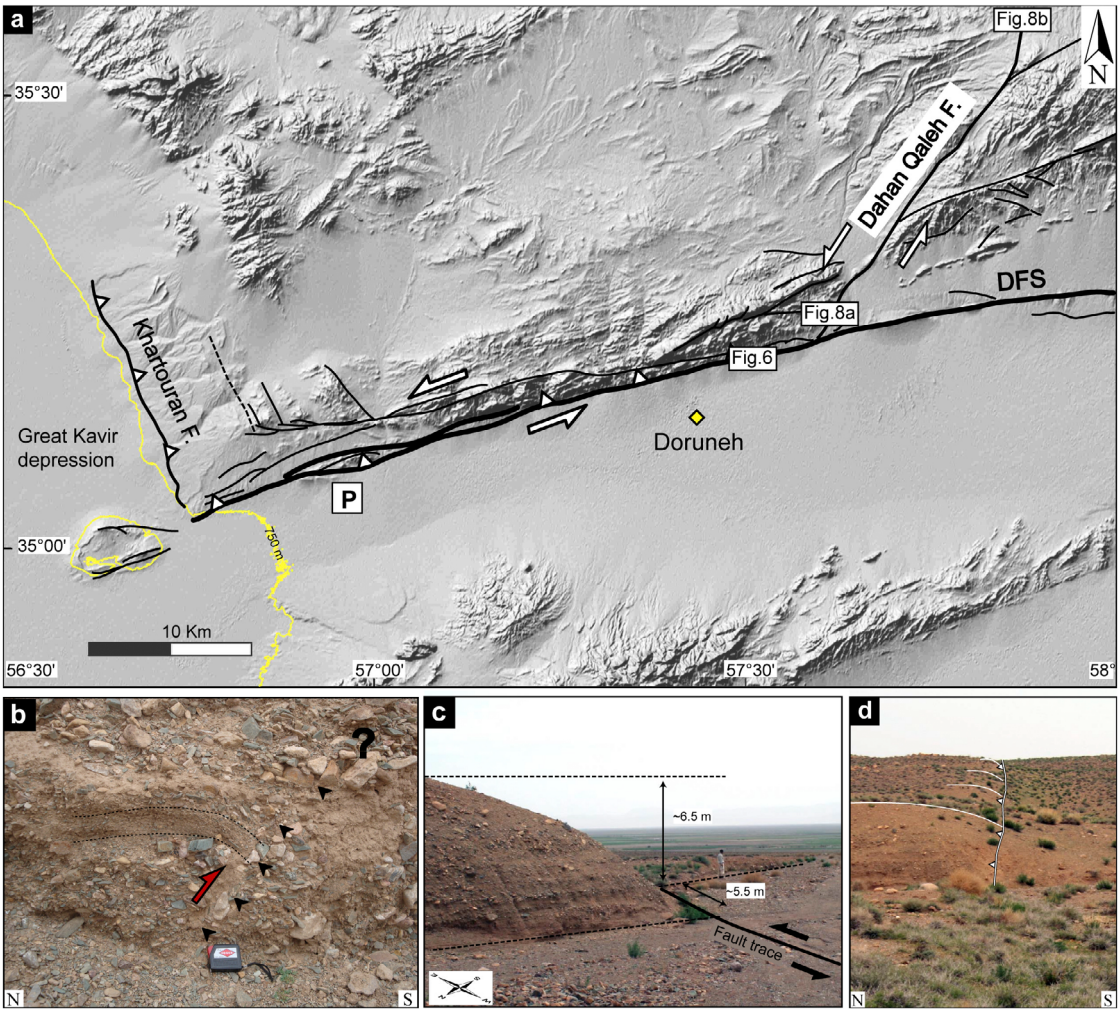

Figure 7. (a) Shaded relief map (SRTM data) of the WFZ. The trace of the WFZ joins at right angle the Kharturan reverse fault zone (KF), which marks a sharp topographic edge at the NE boundary of the Dasht-e Kavir (Great Kavir desert) absorbing the relative westward motion (left-lateral faulting) of the WFZ's northern block. "P" in Figure 7a indicates a pop-up structure formed in a restraining bend along the WFZ. (b) A profile of the fault shown in Figure 7d indicating the reverse component of faulting along the WFZ. (c) Field photograph of a seasonal stream incised in Q1 alluvial fan surface obliquely displaced by the fault indicating coeval vertical and left-lateral offsets of ∼6.5 m and ∼5.5 m. (d) Field photograph of the fault scarp along the WFZ. The accurate locations of field photographs are: Figure 7b, 35.2205°N–57.5577°E; Figure 7c, 35.22106°N–57.5603°E; and Figure 7d, 35.2210°N–57.5606°E.

nearly parallel, and each segment is totally overlapped by one or more nearby fault segments (Figure 5c). In other words, the overlapped length of nearly all segments reaches 100 per cent of the total segment length. Along the central part, overlapping percentage decreases to a mean value of ∼40 per cent (Figure 5c), which means that the involved fault segments are structurally more independent with respect to the fault segments of two other parts.

[18] In summary, the analysis of along-strike variations in the orientation, wideness and geometric arrangement of the DFS leads us to divide the entire fault system into three distinct Western (WFZ), Central (CFZ), and Eastern (EFZ) fault zones (Figure 5a).

4.1.1. The Western Fault Zone (WFZ)

[19] The 85-km-long WFZ comprises nine main strands forming a fault zone of several hundred meters to 2.5 km in width. Left-lateral component of faulting along its left-stepping arranged fault segments forms pull-apart troughs within releasing segment offsets (Figure 6). The western and eastern terminations of the WFZ are marked by two fault zones intersecting the DFS. To the west, the WFZ is intersected at a right angle by a ∼N160°E-trending reverse fault zone (Kharturan) beyond which, except for diffused minor faulting, the surface expression of the DFS is died out (Figure 7). The Kharturan fault zone forms the western boundary of uplifted areas on the northern side of the DFS, where Neogene and Quaternary deposits have been tilted and uplifted against the western playa (i.e., Dasht-e Kavir). On the western side of the Kharturan fault zone, the Dasht-e Kavir (Great Kavir) depression reaches its lowest (750 m) elevation (Figure 7). These structural and geomorphic relationships suggest that the relative westward (left-lateral)

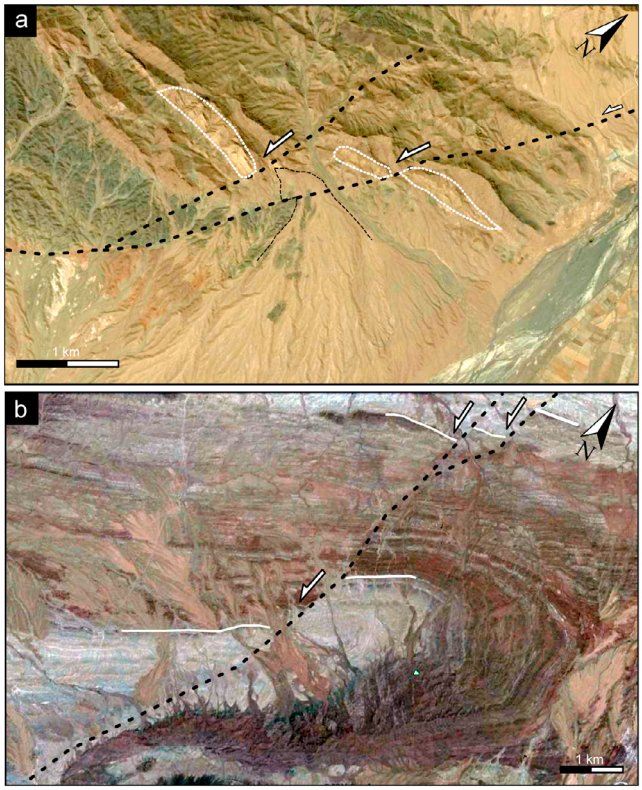

Figure 8. Geomorphic and geological evidence of left-lateral faulting along the Dahan-Qaleh Fault (Quickbird image from GoogleEarth). (a) Cumulative left-lateral offset along the fault running through folded rock units and Quaternary landforms. (b) Left-lateral displacement of the fault in the folded Neogene deposits. Trace of the fault is shown by dotted black lines. White lines marks offset markers. See Figure 7 for the location.

motion of the northern block of the DFS should be principally taken up by reverse faulting along the Kharturan fault zone. Such a mechanism can explain the topographic contrast between the western and eastern sides of the reverse Kharturan fault zone, the die-out of the DFS surface expression, as well as the location of the deepest part of the Dasht-e Kavir playa. If is accepted, the focal mechanism of the 09 December 1979 earthquake, which indicate reverse faulting with little right-lateral component on a NNW-trending nodal plane (section 3), can be representative of a seismic event on the reverse Kharturan fault zone at the western termination of the DFS (Figure 3).

[20] To the east, the western fault zone is intersected by a ~N50°E-trending fault zone (Dahan-Qaleh) which runs NE over a length of ~50 km (Figures 7 and 8). Cumulative offsets recorded by both well-stratified geologic units and geomorphic features (Figure 8) indicate the prominent left-lateral strike-slip character of the fault zone. Eastward from the intersection area, the WFZ joins the central fault zone through a drastic change in the geomorphic expression of the DFS (section 4.2).

4.1.2. The Central Fault Zone (CFZ)

[21] The CFZ runs about 140 km eastward between the longitudes of 57°37′ and 59°15′. The CFZ comprises nine fault strands with lengths ranging from ~5 to 45 km that form a relatively narrow zone of several meters to 400 m in width (Figure 9). Along the CFZ, the frequent structural features are either push-up structures, which were formed within restraining relay zones and/or fault bends, or left-handed pressure ridges formed within stepovers [e.g., *Fattahi et al.*, 2007] or between en echelon fault segments (Figures 9 and 10).

[22] The eastern termination of the CFZ, near the village of Kajderakht, is characterized by a complex structural zone (Figure 10), where, the main fault splits out into the northern and southern strands. The southern strand ends into a ~20-km-long restraining bend comprising SSE-striking reverse faults along which Neogene deposits on the western fault blocks have been thrust over the Quaternary plain on the east side of the faults (Figure 10). In the same area, just south of Torbat-e Heidariyeh, the northernmost strands of the CFZ are intersected by two NNE-trending faults that border a graben-like morphology (Figure 10). There is a striking contrast between geologic outcrops in the inside and outside of the graben (regardless its structural genesis). In the outer side, are Eocene andesitic rocks while in the interior, are middle Oligocene - late Miocene lagoonal to continental sedimentary rocks that have been covered by Quaternary deposits. The inner area is clearly less elevated (~1300 m) than the average elevation (~1650 m) of the uniformly elevated mountains on the other sides of the graben-bounding faults (Figure 10). These geologic and geomorphic features indicate that the graben-bounding faults are two long-lived faults (at least since Early Oligocene), and that together with the southern restraining bend they represent an important boundary condition between the central and eastern fault zones.

4.1.3. The Eastern Fault Zone (EFZ)

[23] The ~140-km-long EFZ forms a horsetail structure or nearly more, a trailing contractional imbricate fan [e.g., *Woodcock and Fischer*, 1986] at the eastern termination of the DFS (Figure 11a). The fault zone varies between 1.5 and 14 km in width, and comprises at least fifteen NE-dipping reverse faults along which Neogene to Quaternary deposits are thrusted over the Holocene plain (Figure 11b). The imbricate reverse faults diverge toward the southeast, and some of them bound the southwest flanks of NW-trending anticlines formed on the hanging wall of the faults (Figure 11c).

4.2. Variations in the Geomorphology and Fault Behavior of the DFS

[24] Given that the rate and kinematics of slip on a Quaternary fault is expressed in the geomorphology of the fault, along-strike variations in the fault behavior could be examined thanks to systematic changes expressed by geomorphic features affected by the fault. The surface trace of the DFS is marked by geomorphic features such as Quaternary alluvial fans and their associated streams that have been laterally and/or vertically offset along the whole length of the fault. Detailed geomorphic mapping based on SPOT5 satellite images complemented by field observations allowed us to subdivide multiple generations of alluvial fans, which are abandoned and entrenched, into Q3, Q2 and Q1 geomorphic surfaces, from upper to lower. Each geomorphic surface exhibits specific geomorphology such as geomorphic

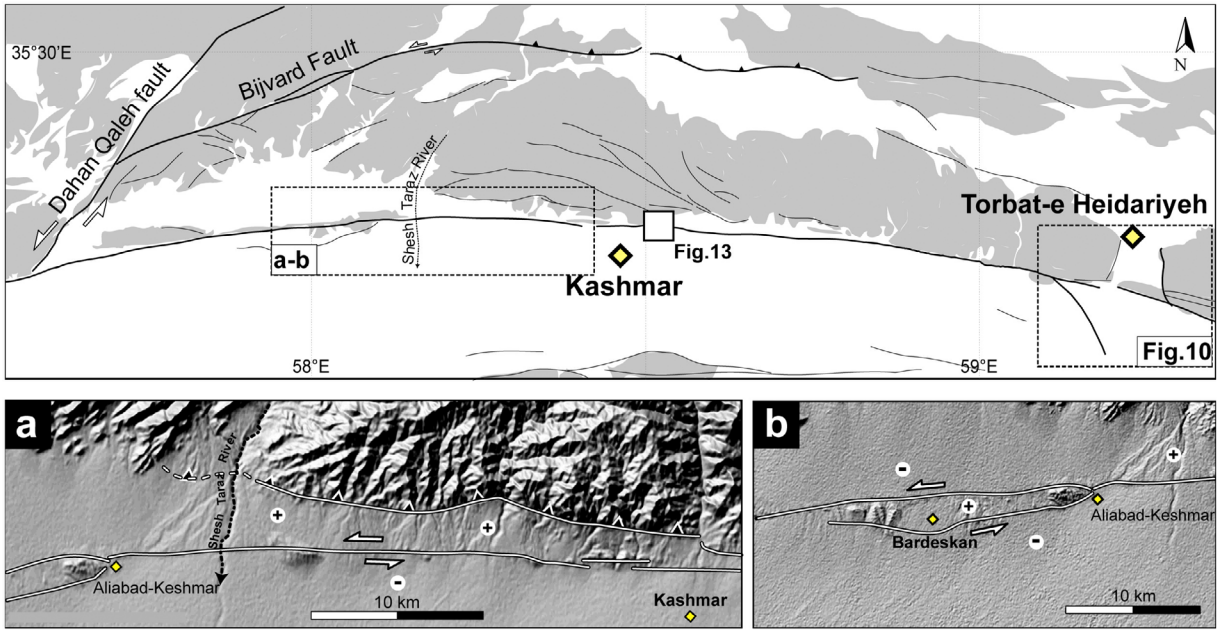

Figure 9. Simplified fault map of the CFZ and the surrounding areas. (a and b) Shaded relief maps based on SRTM digital topographic data indicating two examples of uplifted areas along the CFZ; the uplifted and subsided areas are marked by plus and minus signs, respectively.

terracing (stepping), incision pattern and the state of preservation. Naturally, the higher surfaces are more incised and consequently, less preserved relative to the lower fan surfaces. The type (vertical, horizontal or oblique) and amount of fault offsets recorded by alluvial fans vary along the strike of the fault system such that alluvial fans of the same generation, but in different structural setting, exhibit various type of fault offsets ranging from pure vertical (reverse) to pure horizontal (left-lateral). For instance, the cumulative geomorphic offsets observed along the western and central fault zones imply the respective oblique-slip (reverse left-lateral) and strike-slip (left-lateral) characters of faulting; whereas within the eastern fault zone offsets are principally vertical.

[25] In order to illustrate spatial variations in the amount of lateral offsets recorded by Q1, Q2, and Q3 fan surfaces, cumulative offsets measured along the DFS were plotted versus along-strike distance from the western termination of the fault system (Figure 5d). The amount of cumulative left-lateral offsets systematically increases from the western to the central fault zones. For each fan generation, the largest left-lateral offsets have been recorded by Q3 (840 $\pm$ 70 m), Q2 (400 $\pm$ 10 m) and Q1 (95 $\pm$ 20 m) fan surfaces along the CFZ. But, along the WFZ, cumulative left-lateral offsets recorded by the same fan generations decrease in 240 $\pm$ 40 and 145 $\pm$ 20 m for Q3 and Q2 surfaces, respectively (Figure 12 and Table 2). The only systematic left-lateral offset in Q1 fan surfaces are offset of $\sim$5.5 m recorded by streams incising Q1 fan surfaces. Such an offset value should be considered as a minimum offset along the WFZ (Figure 7c).

[26] The maximum left-lateral offset along the CFZ is recorded by the Q3 Quch Palang alluvial fan [*Wellman*, 1966; *Giessner et al.*, 1984]. In that area, a $\sim$800 m left-lateral offset was measured by *Fattahi et al.* [2007]. Subsequently, the offset value has been reduced to $\sim$150 m by *Walker and Fattahi* [2011] favoring a much smaller displacement which satisfies the IRSL $\sim$50 ka ages [*Fattahi et al.*, 2007] estimated for the uppermost part of fan deposits. This offset reduction is based on a suggestion that assign deposits from a Q2 and another Q3 fan on the south and north sides of the fault, respectively, to remnants of the Q3 Quch Palang fan surface [see *Walker and Fattahi*, 2011]. But, our detailed geomorphic mapping based on the high-resolution Quickbird and SPOT5 imageries complemented by field survey allowed us to define the border of the alluvial fan (Figure 13). The geomorphic reconstruction of both the overall shape of the fan, and mainstreams incised in the fan surface reveals a left-lateral offset of 800 $\pm$ 50 m. The same offset value (880 $\pm$ 50 m) has been obtained through the geometric reconstruction of the axial trace of the fan surface [e.g., *Keller et al.*, 2000; *Shabanian et al.*, 2009a]. This geometric method uses topographic contours of a fan surface to define the geometric axis of the alluvial fan, and avoids producing other possibilities due to interactions between the alluvial fan and other erosional/depositional adjacent features [e.g., *Walker and Fattahi*, 2011]. Interestingly, a topographic profile across the distal part of the Quch Palang alluvial fan clearly reveals the presence of two individual landforms indicating that the lower left part surface (B-B′ in Figure 13) belong to another alluvial fan (Q2 surface). In summary, both the geomorphic and geometric approaches yield a constrained offset of 840 $\pm$ 70 m that is representative of the maximum cumulative left-lateral displacement along the DFS since the abandonment of the Q3 Quch Palang alluvial fan.

[27] Along the CFZ, the largest left-lateral offset (95 $\pm$ 20 m) recorded by Q1 alluvial fan surfaces is observed in Zarmehr area (Site 15 in Figure 12). Previously, a smaller offset of $\sim$25 m recorded by the Q1 Shesh Taraz alluvial fan

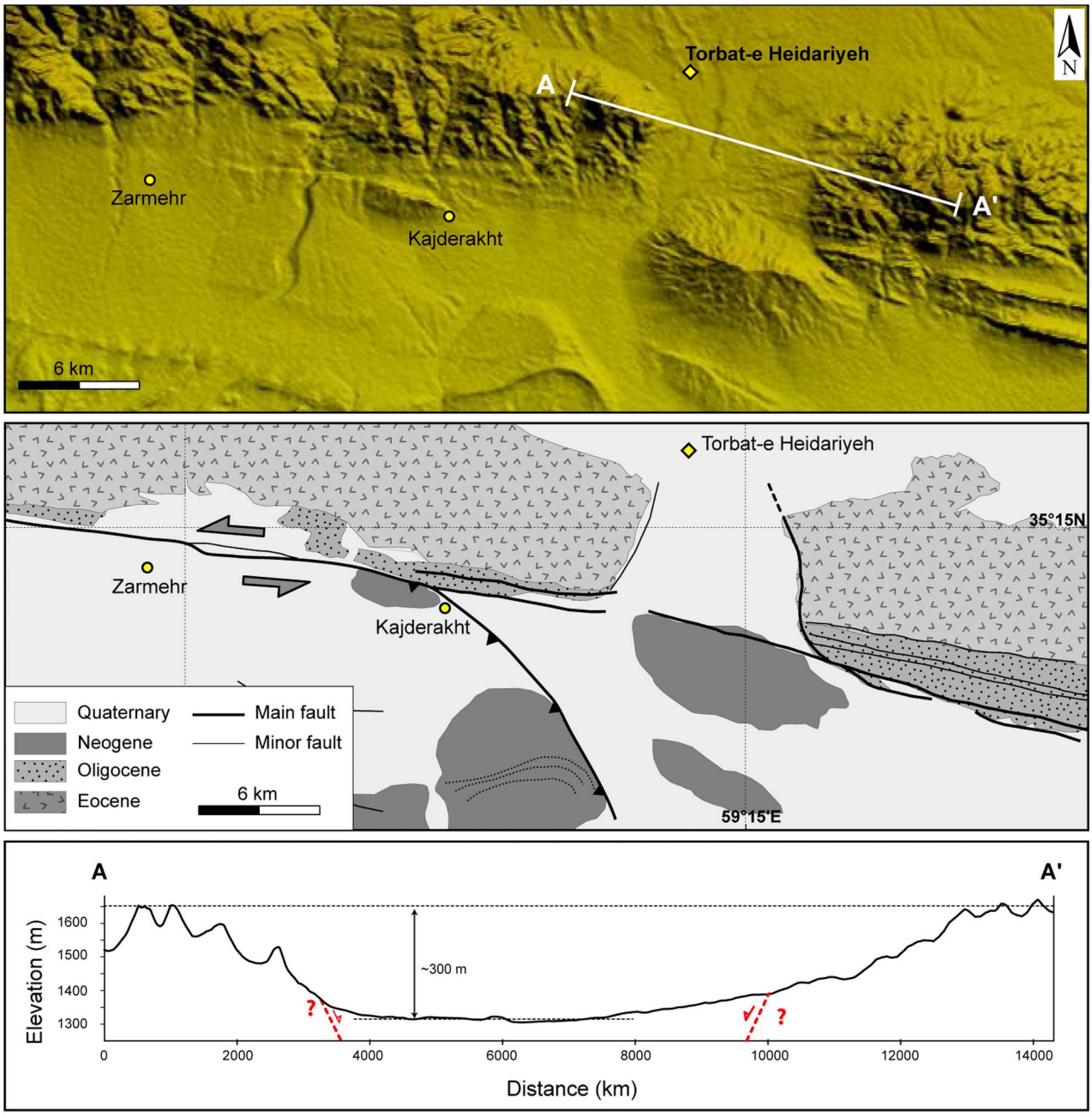

Figure 10. Shaded relief map (SRTM digital topographic data) and simplified morphotectonic interpretation (below) of the eastern termination of the CFZ. The lower topographic profile (white line in Figure 10) represents abrupt topographic changes across the fault-bounded graben (see section 4.1.2 for explanations) at the CFZ's eastern termination.

was reported by *Fattahi et al.* [2007]. The ~25 m offset was suggested to be representative of cumulative offset in Q1 alluvial surfaces along the CFZ [*Fattahi et al.*, 2007; *Walker and Fattahi*, 2011], and has been used to estimate the slip rate of the Doruneh Fault. Actually, the ~25 m offset of T1–T2 riser indicated by *Fattahi et al.* [2007, Figure 8] is clearly an apparent offset resulted from lateral erosion of the riser near the fault trace, and within the eastward continuation of the pull-apart basin (Figure 14). Just ~50 m to the south of the southern fault trace, the T1–T2 riser return back to its initial position such that no left-lateral offset in this riser is observed (Figure 14). Immediately east of the T1–T2 riser there is an older linear riser that does not show any left-lateral offset (Figure 14). Given such relationships, the ~25 m offset deduced from the DGPS-derived topographic map by *Fattahi et al.* [2007] is an apparent offset that cannot be representative of either cumulative or minimum left-lateral offset of the Shesh Taraz Q1 fan surface.

[28] For the eastern fault zone, cumulative displacements are principally vertical, and no conspicuous evidence of lateral faulting is observed. The cumulative vertical displacements are expressed in uplifted and/or tilted Quaternary

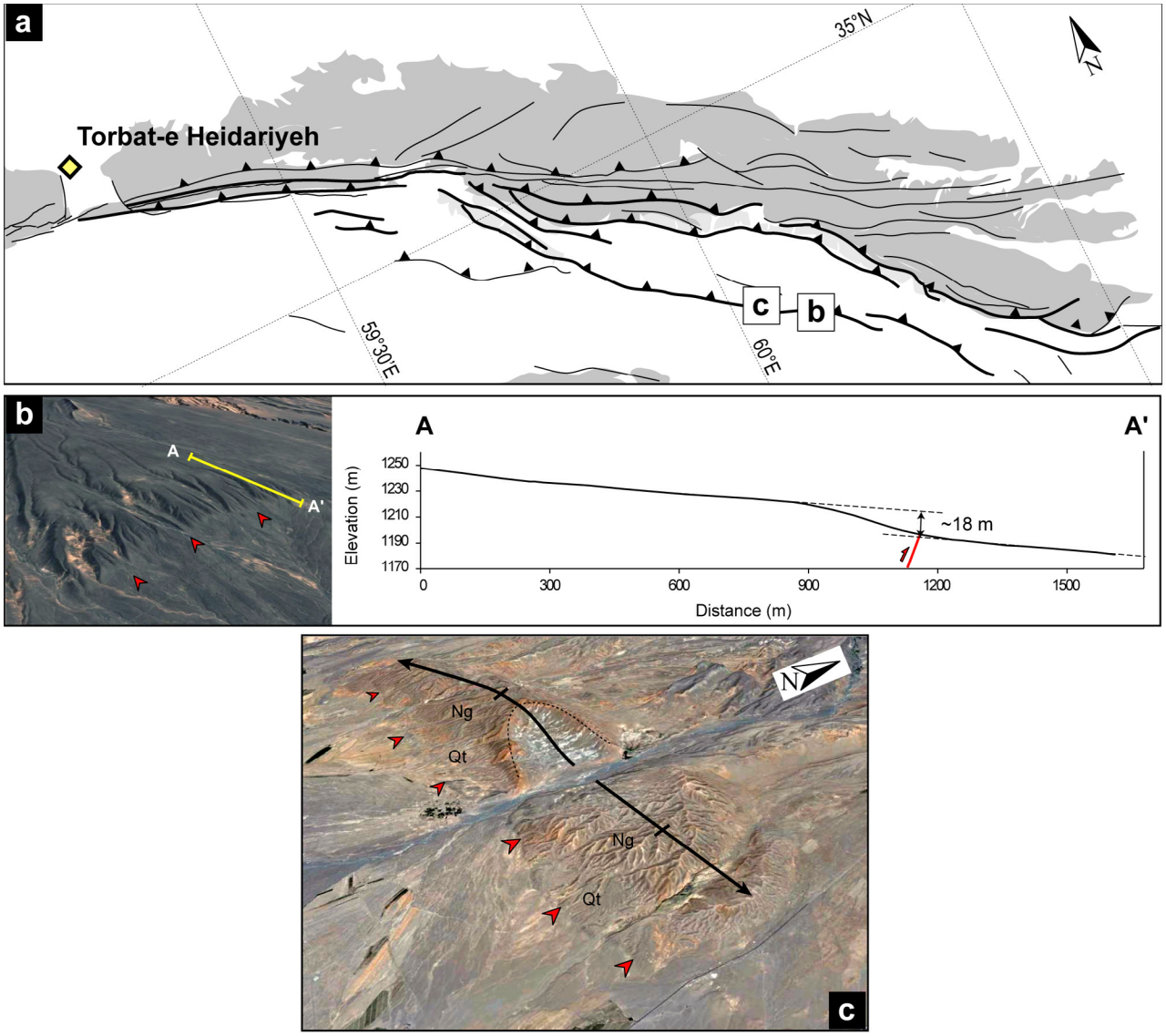

Figure 11. (a) Fault map of the EFZ. Quaternary fault traces are shown by thick black lines. Faults along which there is no evidence of Quaternary activity are marked by thin black lines. (b) Three-dimensional view (Quickbird image superposed on SRTM data from GoogleEarth) of a Q_3 alluvial fan that has vertically been offset on a fault within the EFZ. A topographic profile (A-A′ in Figure 11b), based on SRTM data, that illustrates vertical faulting along the westernmost fault of the EFZ. (c) A growing anticline (3D view from GoogleEarth) on the hanging wall of a reverse fault of the EFZ. Quaternary deposits were titled and uplifted on the SW flank of the fold. The trace of the fault is indicated by triangles.

surfaces on the hanging wall of reverse faults or on the fault-bounded flanks of probably fault-related anticlines (Figures 11b and 11c). The lack of left-lateral displacement in the eastern part of the DFS, thus, suggests that strike-slip faulting along the CFZ is principally taken up by reverse faulting and the associated folding along the EFZ within a trailing contractional imbricate fan structure (Figure 11).

[29] Assuming that alluvial fan surfaces belong to each generation of Q1, Q2, and Q3 geomorphic surfaces were abandoned at the same time; spatial variations in the type and amount of cumulative offsets recorded by the fan surfaces represent along-strike changes in the kinematics and slip rate of the DFS. This assumption was examined at one site along the eastern part of the WFZ (Figure 7). In that area, multiple generations of alluvial fans and streams have been offset by the fault providing evidence of both reverse and left-lateral fault displacements. A Q1 fan surface has recorded a minimum vertical offset of ~6.5 m that is coeval with a left-lateral offset of ~5.5 m (Figure 7c). Our measurement on the fault plane, which is crop out in the left bank of the axial stream of the fan (Figure 7b), indicates geometry of N73°E/65°NW, and allows determining a geomorphic-derived pitch angle of ~50°NE for the main strand of the WFZ. This pitch angle is clearly higher than the average pitch angle (15 ± 5 degrees) we measured along the CFZ (section 5.2). Such a direct observation explain why the cumulative horizontal offsets recorded by Q3, Q2, and Q1 fan surfaces affected by the western fault zone are

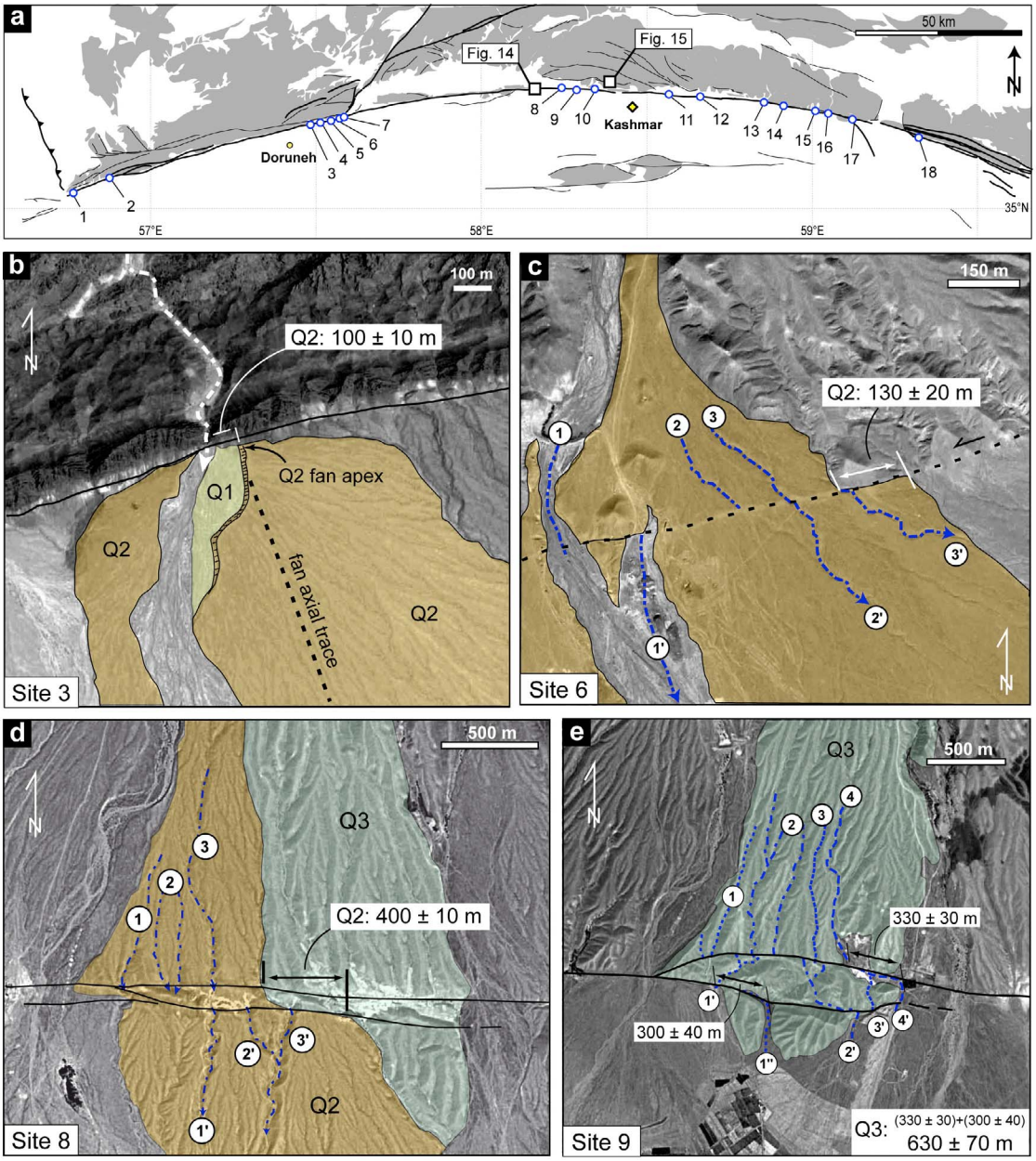

Figure 12. (a) General fault map of the DFS showing the location of sites in which left-lateral offset recorded by Q1, Q2, and Q3 alluvial fans have been measured. The most important offset measurements, which have a crucial role in the understanding of offset variations along the DFS, are shown in Figures 12b–12i. (b) A Q2 fan apex left-laterally offset along the WFZ. (c) The eastern boundary of a Q2 alluvial fan offset along the WFZ. (d) The Q2/Q3 terrace riser left-laterally offset along the CFZ representing the cumulative offset of the Q2 fan surface. (e) An eroded Q3 alluvial surface left-laterally offset along the CFZ. The initial shape of the alluvial fan cannot be reconstructed. A 630 ± 70 m cumulative offset (sum of two offset along the northern and southern fault strands) recorded by streams incising in the fan surface have been measured as a minimum left-lateral offset at site 9. Note that each beheaded stream in the northern side has been compared with the first stream on the left in the southern side. (f) Streams incised in a Q2 fan surface have recorded a minimum cumulative offset of the surface. The Q1/Q2 terrace riser reveals the cumulative left-lateral offset recorded by the Q1 fan surface. The middle part of the fault strands is a pressure ridge. (g) Streams incised in Q2 alluvial surfaces recorded left-lateral offset of 150 ± 30 m along the CFZ. (h) Q3 alluvial surfaces offset along the easternmost of the CFZ. The same left-lateral offset is shown by drainages on the left of the Q3 surface. The (1′) stream segment is abandoned due to the fault offset. (i) Terrace riser between Q1 and Q2 alluvial fan surfaces has been offset along three strands of the CFZ indicating the offset recorded by the Q1 fan surface.

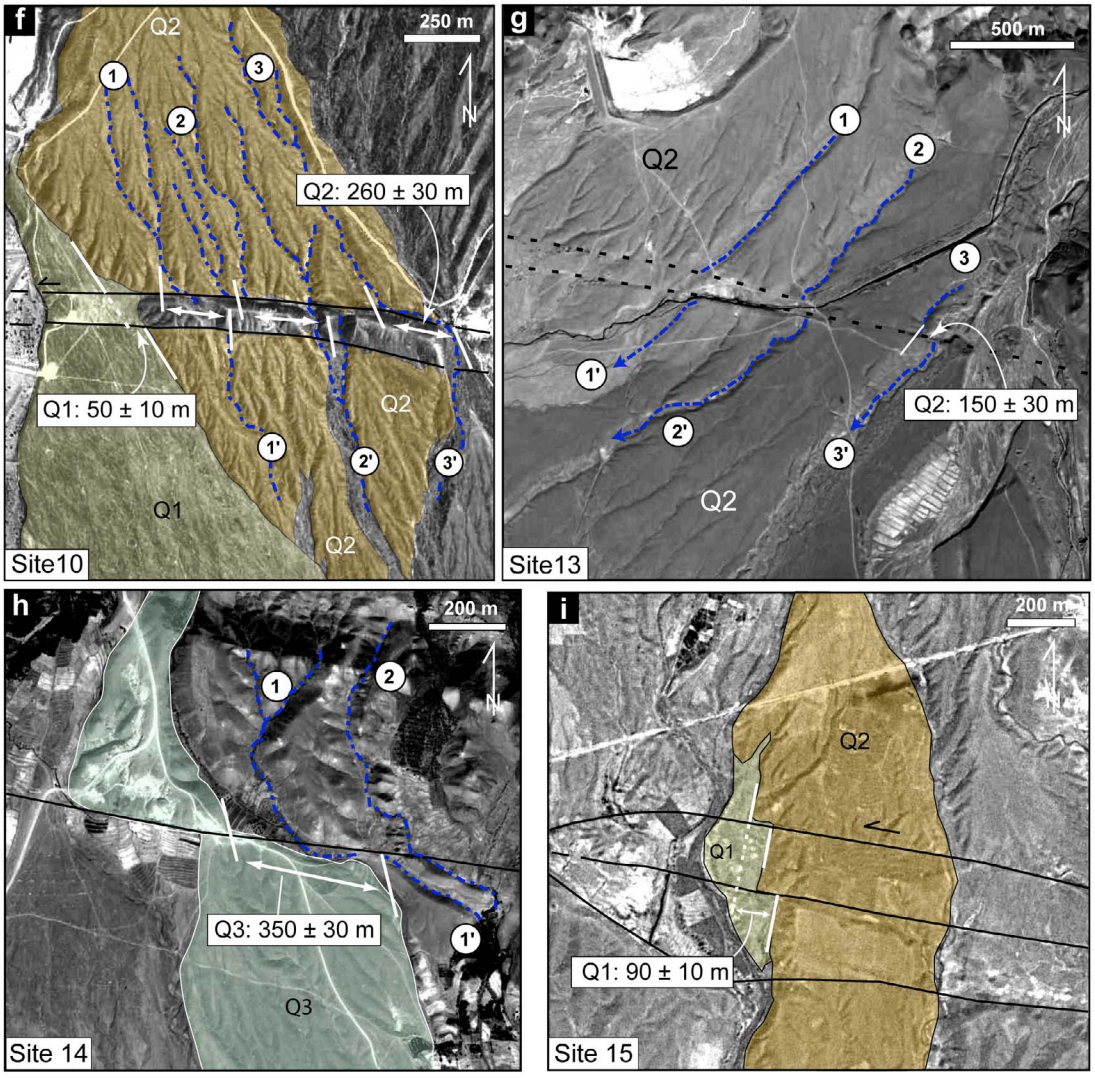

Figure 12. (continued)

significantly less than offsets recorded by the equivalent fan surfaces along the central fault zone.

[30] On the other hand, we showed that (Figure 5d) systematic variations in cumulative fault displacements correspond with changes in the geometry and structure of the fault system. Altogether, the consistency between long-lived geomorphic, structural and behavioral fault characteristics indicate the persistence of the fault zone boundaries using which the DFS is divided into three distinct western, central and eastern fault zones.

5. The Present-Day Kinematics and Seismic Potential of the Central Fault Zone

[31] The CFZ accommodates the E-W shear between the north and south tectonic domains of the DFS by pure left-lateral strike-slip faulting. The region affected by the CFZ is the place of populated large towns such as Kashmar, Bardeskan and Torbat-e Heidariyeh. We conducted more detailed geomorphic and structural investigations along the CFZ to describe the kinematics of active faulting and to reevaluate the seismic potential of the fault zone.

5.1. The CFZ: An Oblique-Slip or Strike-Slip Fault Zone?

[32] The present-day kinematics of the DFS has been under debate because of ambiguous geomorphic features such as Quaternary fault escarpments, with height of several tens of meters, especially along the central part of the fault system [e.g., *Tchalenko et al.*, 1973; *Mohajer-Ashjai*, 1975; *Fattahi et al.*, 2007]. On the other hand, a lack of focal mechanism of earthquake that can be directly assigned to the DFS (see section 3) precludes previous workers to describe the active kinematics of the fault.

[33] In the pioneer works by *Tchalenko et al.* [1973] and *Mohajer-Ashjai* [1975], the uplift domains in either sides of the fault were interpreted as the geomorphic expression of vertical displacements, whatever their sense, on south-dipping steep fault planes. Nevertheless, the distribution of these areas on both side of the fault precluded the previous workers to conclude about the normal or reverse character of faulting. For instance, based on the basin-ward emplacement of younger alluvial fans with respect to older fan surfaces (between Kashmar and Nay), *Tchalenko et al.* [1973]

Table 2. Geomorphic Offset Measurements Along the DFS[a]

Site Name	Fault Zone	Latitude (°E)	Longitude (°N)	Quaternary Measured Surface		
				Q3	Q2	Q1
1	WFZ	35.0389	56.7664	-	20 ± 10	-
2	WFZ	35.0762	56.8763	-	60 ± 10	-
3	WFZ	35.2015	57.4409	-	100 ± 10	-
4	WFZ	35.2076	57.4835	-	145 ± 20	-
5	WFZ	35.2173	57.5456	240 ± 40	-	-
6	WFZ	35.2232	57.5713	-	130 ± 20	-
7	WFZ	35.2255	57.5833	-	130 ± 20	-
8	CFZ	35.2976	58.2422	-	400 ± 10	-
9	CFZ	35.2933	58.2878	630 ± 70	-	-
10	CFZ	35.2962	58.3432	-	260 ± 30	50 ± 10
11	CFZ	35.2825	58.5676	840 ± 70	-	-
12	CFZ	35.277	58.6623	-	300 ± 50	100 ± 15
13	CFZ	35.2622	58.855	-	150 ± 30	-
14	CFZ	35.2542	58.9131	350 ± 30	-	-
15	CFZ	35.241	59.009	-	-	90 ± 10
16	CFZ	35.235	59.049	-	190 ± 30	-
17	CFZ	35.221	59.12	330 ± 20	-	-
18	EFZ	35.175	59.3226	-	60 ± 10	-

[a]Site name refers to the numbers marked in Figure 12a. The most important offsets playing a crucial role in offset variations along the DFS are presented in the Figures 12b–12i.

proposed episodic vertical (normal) movements elevating the northern block (mountain side) relative to the southern side (alluvial basin), and consequently, to push younger alluvial fans being formed downhill from the fault zone. On the other hand, the presence of an elevated ridge south of the fault zone between Nay and Azghand led *Mohajer-Ashjai* [1975] to propose a reverse fault kinematics associated with a minor component of left-lateral faulting.

[34] Our detailed mapping of Quaternary alluvial fans reveals that the distribution of alluvial fans does not follow the pattern suggested by *Tchalenko et al.* [1973]. In the Quch Palang area, for example, the lowest fan surface (Q1), above the active streambed, was formed south of the fault zone and has not been affected by the fault activity. Further west (~2 km), another Q1 fan spread on the both sides of the fault zone and is left-laterally offset along two fault strands. In that area, there is no evidence of vertical fault displacements on the fan surface (Figure 13). The same conclusion has been reached by *Fattahi et al.* [2007] reporting little (~1.5–2 m) vertical displacement recorded by a Q1 alluvial fan at the outlet of the Kashmar River.

[35] Indeed, it is difficult to determine the sense of vertical movements only based on the arrangement of locally uplifted domains which are randomly distributed along a fault trace, especially when the dip direction of the fault is unclear. Other confusing geomorphic features interpreted as vertical offsets along the DFS are topographic steps in Q2 and Q3 alluvial fan surfaces [*Tchalenko et al.*, 1973; *Fattahi et al.*, 2007] which are frequently observed on the northern side of the fault (Figures 9a and 9b). These features, in most cases, are apparent fault escarpments when the fault transects rugged topography produced by lateral stepping alluvial fans that are alternated by erosional domains of large streams. In such morphology, the displaced part of the alluvial fans located on the southern side of the fault was missed due to ongoing erosion and/or sedimentation such that the counterpart of the fan appears as a linear escarpment. This suggestion is testified by the fact that along the same fault trace there are other fan surfaces which have left-laterally been displaced keeping their counterparts, whereas, there is no evidence of significant vertical displacements across the fault trace (Figure 13a).

[36] In some cases, interaction between adjacent faults also leads to relatively large uplift domains. For instance, between Kashmar and Ali Abad Keshmar village, the central fault zone is intersected by a NNE-dipping reverse fault that cuts Quaternary deposits at the Siah-Kuh Mountain front (Figure 15). The combination of left-lateral faulting along the DFS and oblique-slip reverse faulting along the NNE-dipping reverse fault forms a narrow contractional wedge (Figure 9a) within which alluvial fan surfaces have been uplifted and intensely eroded.

[37] In summary, such an irregular uplift pattern indicates the strike-slip characteristics of the fault zone along which the position and orientation of local domains of extension and compression, and related geomorphic features depends on the bending and stepping geometry of the strike-slip fault zone, as well as the degree of transpression or transtension [e.g., *Sylvester*, 1988].

[38] Interestingly, our fault kinematic measurement (section 5.2) along the central part of the DFS represents steep fault planes with low pitch angles ranging from 10 to 20 degrees, indicating the pure strike-slip character of the CFZ (Figure 16c). Nevertheless, structural complexities such as releasing and restraining stepovers and/or bends cause different styles of deformation producing a large variety of shortening and stretching domain.

5.2. Modern Stress State Along the CFZ Deduced From Fault Kinematic Analyses

[39] Fault slip data consisting of fault planes and associated striations were measured in five localities distributed along the CFZ (Figure 16). The inversion of fault kinematic data has been performed using the method originally proposed by *Carey* [1979]. This fault kinematics inversion method computes a mean best fitting deviatoric stress tensor from a set of striated faults by minimizing the angular deviation (misfit angle) between a predicted slip vector and the observed striation [*Carey and Brunier*, 1974; *Carey*, 1979]. In all fault kinematic inversion schemes, the main assumption is that slip direction indicated by the striation represents the direction of the shear stress resolved on the fault plane. The inversion results include the orientation (trend and plunge) of the principal stress axes ($\sigma1 > \sigma2 > \sigma3$, corresponding to maximum, intermediate and minimum stress axes, respectively) of a mean deviatoric stress tensor as well as a stress shape parameter $R = (\sigma2 - \sigma1)/(\sigma3 - \sigma1)$ that describe relative stress magnitudes ranging from 0 to 1 [e.g., *Carey and Brunier*, 1974; *Bellier and Zoback*, 1995; *Shabanian et al.*, 2010, and references therein].

[40] At two of five sites, fault slip data were measured in Quaternary alluvial fan deposits, while at the three other sites measurements were made in Eocene and Neogene rocks (Figures 16a and 16b and Table 3). Fault slip data comprising fault slip families belonging to two different tectonic regimes was manually separated into appropriate data sets. The data separation was done on the basis of geological field data using relative chronology of the striations (crosscutting relationships).

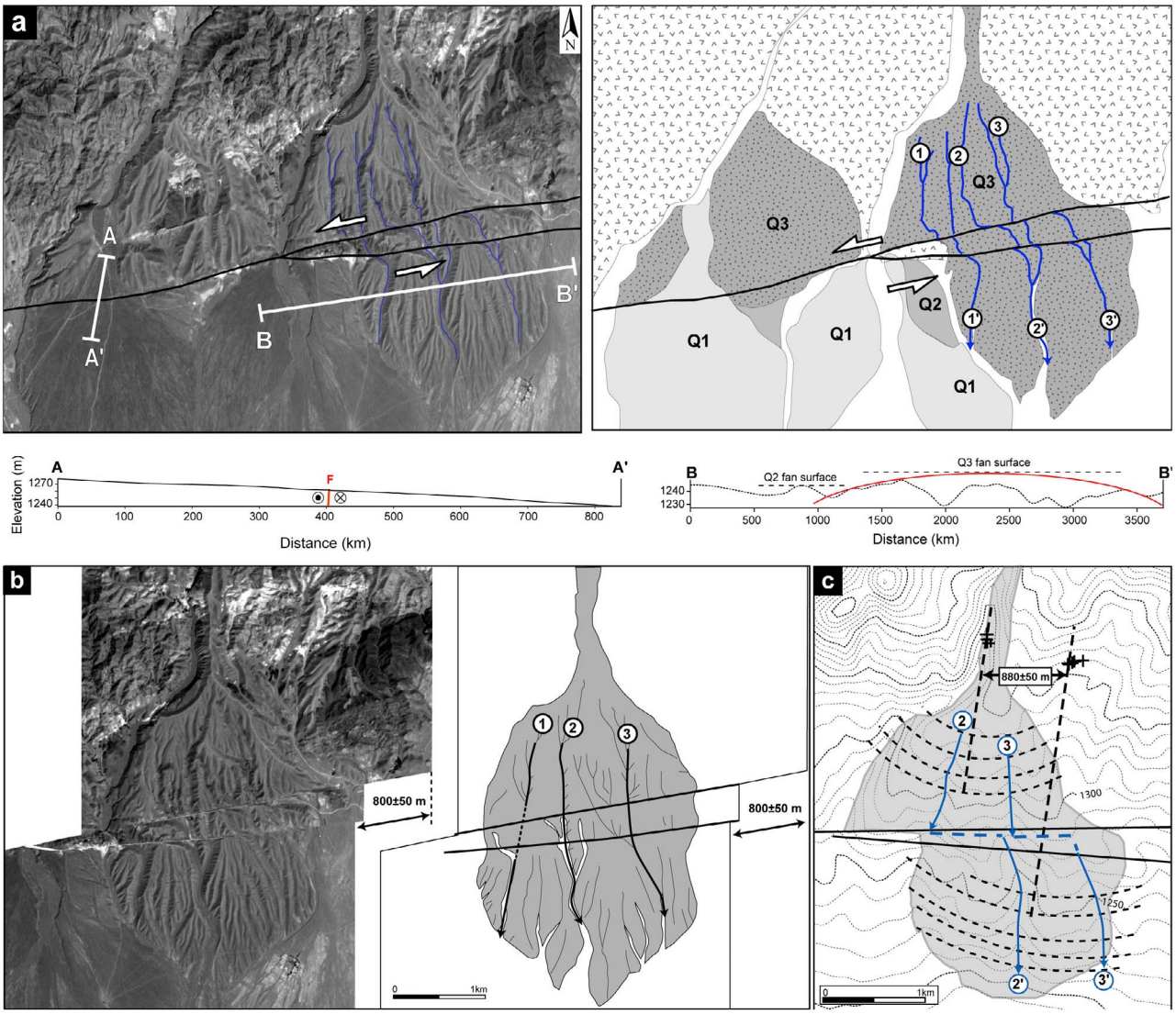

Figure 13. (a) SPOT5 image and its morphotectonic interpretation centered on the Quch Palang area which shows the geomorphic setting of Q3 and Q1 alluvial fans along the CFZ. A-A′ topographic profile on a Q1 fan surface shows that there is no vertical displacement across the fault cutting the Q1 fan surface. B-B′ topographic profile across the Q3 Quch Palang alluvial fan indicates the topographic difference between the Q3 and Q2 geomorphic surfaces. (b) The geomorphic reconstruction of both the overall shape and mainstreams of the Quch Palang alluvial fan. (c) The geometric and topographic reconstruction of the Quch Palang fan. The location of apex defined using concentric arcs on the distal part of the fan is located ~880 m to the east of the initial apex. This offset value is the same than the offset recorded by mainstreams incising in the fan surface.

[41] The modern stress state was determined using the youngest striae sets measured in both pre-Quaternary rock units and Pleistocene conglomerates (Figure 16a and Table 3). For all data sets, the calculated modern stress tensors are coherent regardless ages of the rocks in which fault slip data were measured. The modern stress state is characterized by a N45 ± 15°E-trending $\sigma 1$ and shows a predominated strike-slip tectonic regime, except for one site with compressional tectonic regime (site 2, Figure 16a).

[42] The inversion analysis is individually performed for the oldest striae sets measured in pre-Quaternary rock units (Figure 16b and Table 3). The calculated paleostress tensors represent a N150 ± 20°E-trending $\sigma 1$, with a compressional tectonic regime.

[43] Applying the average N45°E-trending horizontal $\sigma 1$ (modern stress) to average geometry (N95 ± 5°E) of the CFZ implies dominant left-lateral strike-slip faulting, which is consistence with late Quaternary geomorphic expression of the fault zone. Both the modern and paleostress states we computed are compatible with corresponding stresses axes in NE Iran, which were deduced from the inversion of both geologically and seismically (in the case of modern stress

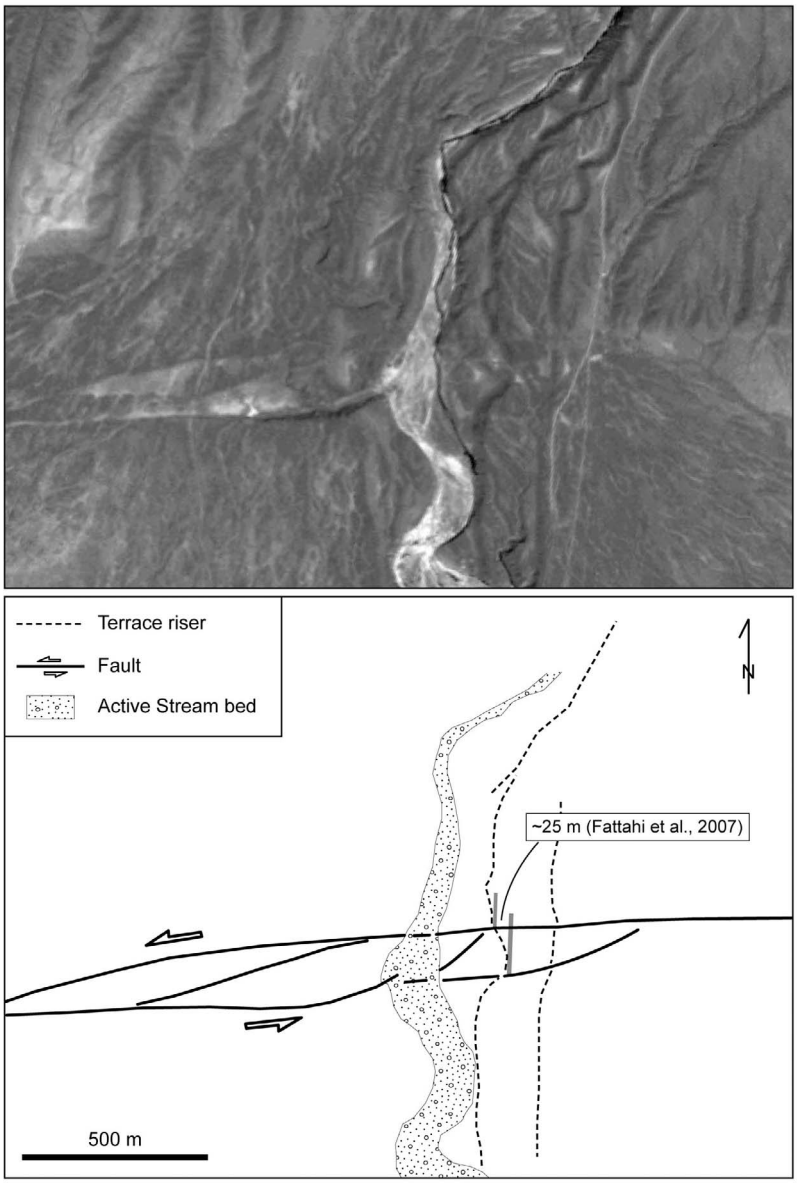

Figure 14. The ~25 m cumulative offset in Q1 alluvial surfaces along the Sheh Taraz river west of Kashmar reported by *Fattahi et al.* [2007]. See text for more information and Figure 12a for the location.

state) determined fault slip vectors [*Shabanian et al.*, 2010; *Javidfakhr et al.*, 2011].

5.3. Seismic Potential of the Central Fault Zone

[44] The CFZ is presumably a hazardous fault zone that is favorably oriented for movement in the present-day stress field, and could produce damaging large ($M \geq 7$) earthquakes [e.g., *Fattahi et al.*, 2007]. Generally, the assessment of earthquake faulting and the associated seismic hazard relies heavily on the assumption that future large earthquakes will occur in the same regions as historical events [*Coppersmith*, 1988; *Adams et al.*, 1995]. Thus, the temporal and spatial distribution of past earthquakes in addition to the knowledge of active faulting have been the principal sources of information used to forecast where large events will likely occur in the future. In the region affected by the CFZ, however, a lack of adequate historical and instrumental records of seismicity has been a fundamental obstacle in the way of both the deterministic and probabilistic approaches of seismic hazard assessments.

[45] In spite of this difficulty, the combination of geomorphic, kinematic, and structural characteristics of the CFZ allowed us to evaluate the seismic potential of the fault zone. On one hand, we used the *Wells and Coppersmith* [1994] relation between surface rupture length (SRL for strike-slip faults) and the moment magnitude (M). For this purpose, SRL corresponds to between 50 and 100 per cent of the maximum surface length of the fault [see *Berberian and Yeats*, 1999], which can be reactivated during an earthquake. But, the structural characteristics of the CFZ propose

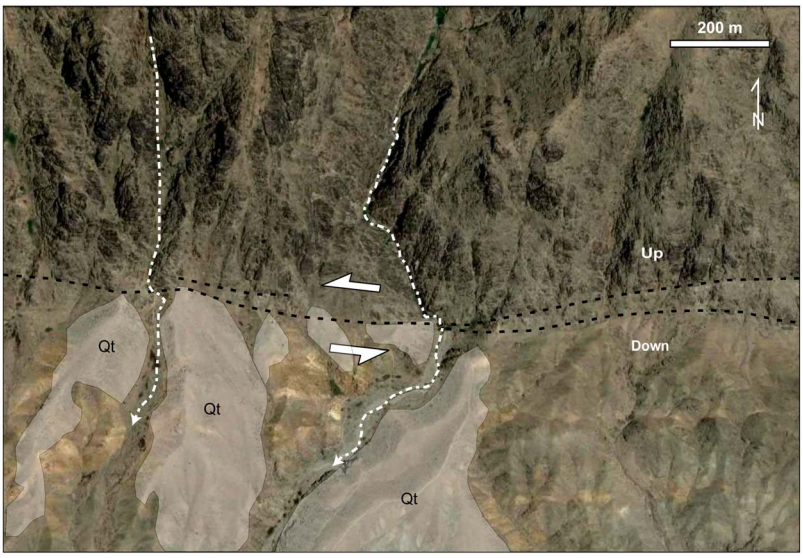

Figure 15. The central part of the N-dipping oblique slip fault at the Siah-Kuh Mountain front in the north of the CFZ. The fault offsets (reverse left-lateral) both Quaternary deposits and south running streams. See Figure 12a for the location.

two possible maximum surface lengths. If we assume that the whole length of the CFZ would reactivate as a single seismogenic fault segment, the total length of 140 km of the fault zone yields a maximum magnitude of 7.2–7.6. While, if each main fault strand of the CFZ represents an independent seismogenic segment, a length of ∼48 km for the longest fault strand consist with earthquakes of $M \leq 7$.

[46] We also analyzed possible coseismic displacements that are found along the fault zone. Around the village of Forsheh (Figure 17), two kariz lines (qanat; traditional Iranian system of irrigation composed of underground canals drawing water from mountain sources by gravity) provide evidence of coseismic fault offsets. East of the Forsheh village, two ∼1-km-apart kariz lines show left-lateral offsets of ∼4 and ∼8 m (Figure 17). The largest offset (∼8 m) corresponds to the kariz line that is suggested to be relatively older given the repaired form of the Karizes (Figure 17b). Further west, between Shesh Taraz and Kashmar, *Fattahi et al.* [2007] found a series of stream offset along the CFZ representing nearly the same offset values averaged at ∼4.7 m. The consistency of these offset values observed at different places along the CFZ may imply a possible characteristic offset [cf. *Schwartz and Coppersmith*, 1984] of ∼4–5 m for the central part of the DFS. If is accepted, the cumulative offset of 8 m could be achieved by successive (recurring) occurrences of two earthquakes of $7.1 \leq M \leq 7.4$ (*Wells and Coppersmith* [1994] relations), which may indicate the reactivation of an independent ∼50-km-long seismogenic fault segment up to a ∼80-km-long fault zone.

[47] The ∼8 m cumulative left-lateral offset along the CFZ may lead also to estimate a possible recurrence interval dividing the time over which the events occurred by the number of earthquakes during that time interval [e.g., *Wallace*, 1970; *Budding et al.*, 1991]. Unfortunately, it is not possible at present to establish the age of the displaced kariz lines. The oldest known kariz in Iran was constructed in the second millennium B.C. at the northern edge of the Dasht-e Kavir [*Wulff*, 1968; *Berberian and Yeats*, 1999, and references therein]. Assuming that the oldest kariz line offset by the CFZ is as old as 4000 yr, the successive occurrence of two seismic faulting events yields a possible maximum recurrence interval of ∼2000 years for large earthquakes of $M \leq 7.4$. Our presumed result seems coherent with that is suggested by *Fattahi et al.* [2007], and may help to characterize the seismogenic behavior of the CFZ. However, in the absence of historical records of large earthquakes along the CFZ we cannot rule out the possibility of creep faulting. Detailed paleoseismological investigations are necessary to differentiate the contribution of seismic and possible aseismic faulting along the DFS. Nevertheless, according to our data and deduced results indicating that the three western, central, and eastern fault zones of the DFS have had distinct evolution history during the Middle to Late Pleistocene, it is unlikely that the "Doruneh Fault" could rupture along the entire ∼600 km length to produce earthquakes of $M \geq 8$.

6. Discussion

6.1. Kinematic Models of the Doruneh Fault System

[48] The geodynamic role of the Doruneh Fault is one of the debates in the active tectonics of the Iranian plateau. Actually, two perpendicular right-lateral (i.e., N-S strike-slip fault systems) and left-lateral (e.g., Doruneh Fault) sets of faults in eastern Iran accommodate crustal shortening in ways that the relationship between the overall convergence vector and slip on strike-slip faults is nearly unclear [e.g., *Allen et al.*, 2006; *Walker and Jackson*, 2004; *Jackson and McKenzie*, 1984]. Both geological [e.g., *Walker and Jackson*, 2004; *Meyer and Le Dortz*, 2007] and geodetic GPS [*Vernant et al.*, 2004; *Masson et al.*, 2005; *Reilinger et al.*, 2006] studies indicate the northward motion of central Iran – Lut relative to Eurasia along N-S strike-slip fault

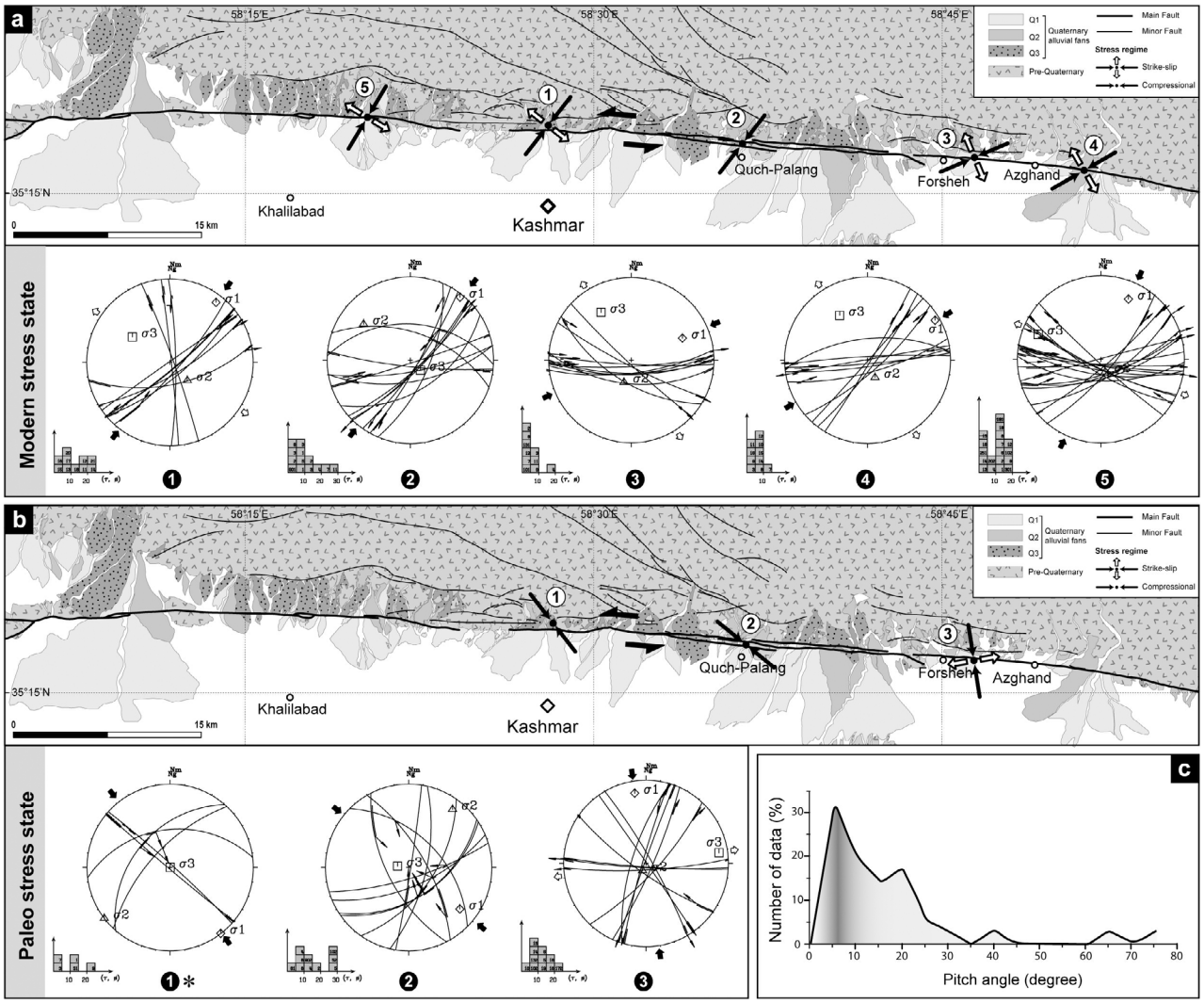

Figure 16. Results of the inversion analysis of fault kinematic data measured along the CFZ. Azimuths of $\sigma 1$ (maximum stress) axis for (a) modern stress and (b) paleostress states are presented on the upper part of each panel. Numbers refer to site names detailed in Table 3. The lower hemisphere stereograms of fault planes and associated slip vectors (arrows on fault planes) together with deduced stress directions (large arrows) are shown on the lower parts. Histograms show distribution of deviation angles between the measured and calculated slip vectors [e.g., *Bellier and Zoback*, 1995]. (c) Distribution of pitch angles measured on main fault planes within and parallel to the CFZ; about 80 per cent of pitch angles are lower than 20 degrees.

Table 3. Result of Stress Tensor Inversion for Slip Data Representing Late Cenozoic Faulting Stress Regimes

			Paleostress					Modern Stress					
			Stress Axis (Trend/Plunge)					Stress Axis (Trend/Plunge)					
Site	Longitude (°E)	Latitude (°N)	$\sigma 1$	$\sigma 2$	$\sigma 3$	R	Rm	$\sigma 1$	$\sigma 2$	$\sigma 3$	R	Rm	Formation Age
1[a]	58.466	35.287	142/00	052/00	322/90	0.57	—	038/06	136/56	304/33	0.95	SS	Eocene
2	58.591	35.280	129/13	037/08	278/75	0.78	C	038/02	308/19	135/71	0.86	C	Neogene
3	58.773	35.270	351/09	206/79	082/06	0.61	SS	067/22	198/58	328/21	0.43	SS	Quaternary
4	58.849	35.264	—	—	—	—	—	060/03	157/65	328/25	0.81	SS	Quaternary
5	58.335	35.294	—	—	—	—	—	031/02	131/78	300/12	0.23	SS	Quaternary

[a]For the fault data populations comprised of less than four well-distributed fault directions, a "fixed" solution [*Bellier and Zoback*, 1995] was applied, in which the principal stress axes are fixed to lie in horizontal and vertical planes. Such deviatoric stress tensors are only used for deducing the direction of principal stress axes, not used for R value interpretation (stress regime). See Figure 9 for the location of sites. Ages are reported from geological maps cited in the text; R, stress shape parameter; Rm, stress regime: C, compressional; SS, strike-slip.

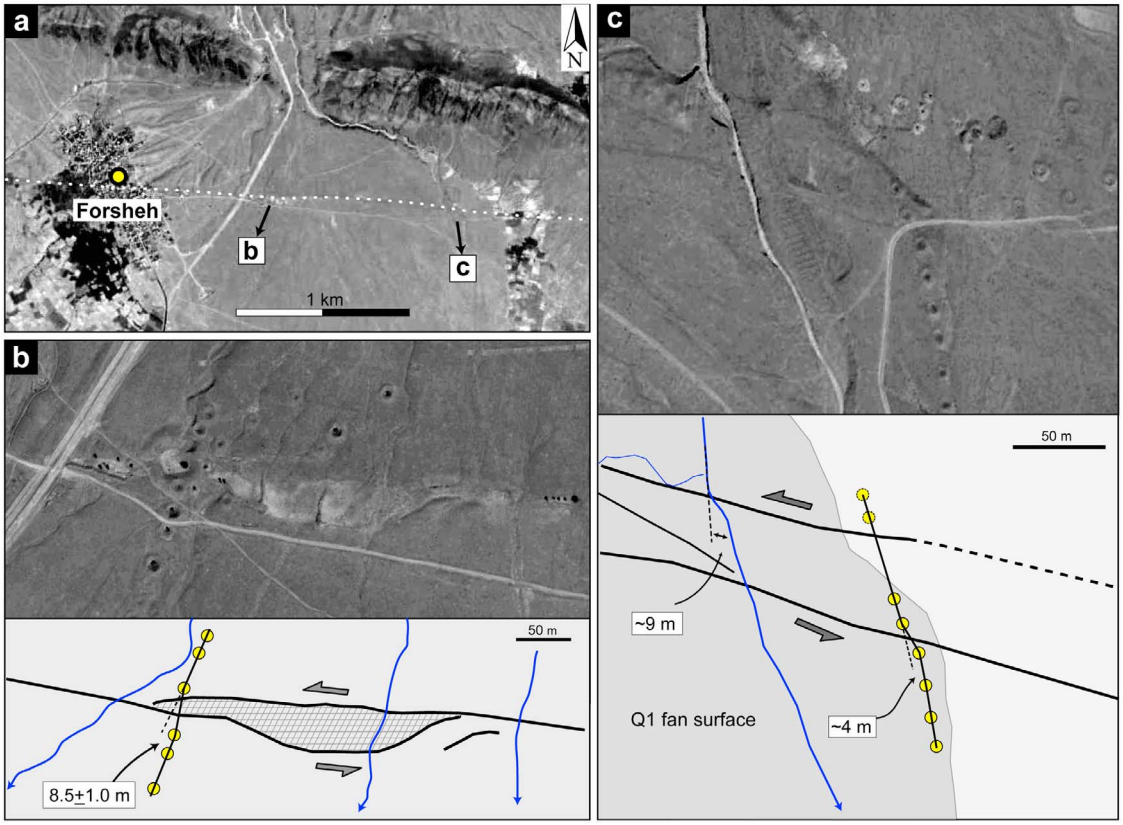

Figure 17. (a) SPOT5 image of a Q1 alluvial fan (east of Forsheh village) affected by the CFZ. Two kariz lines were left-laterally offset along a coseismic rupture zone. (b) The relatively older kariz line is offset of 8 ± 1 m, where a pull-apart through was formed due to left-lateral faulting of the fault. (c) The younger kariz shows an offset of 4 ± 0.5 m. In the same area, along another fault trace, a stream was offset of ∼9 m that is consistent with the offset shown in Figure 17c observed along the northern fault segment.

systems (section 2). While, previous geological works [e.g., *Walker and Jackson*, 2004; *Fattahi et al.*, 2007] have suggested nearly pure left-lateral strike-slip faulting along the entire DFS, which is perpendicular to the overall northward motion of the southern regions (Figure 1). The kinematics of the DFS is controlled by various interplaying factors such as the present-day regional stress state (section 5.2), structural complexities and geometry of the DFS (sections 4.1 and 4.2), as well as kinematic interactions between the DFS and other intersecting fault zones (this section).

[49] A vector addition of GPS-derived velocities at two SHIR and KASH stations [*Masson et al.*, 2007] indicate an overall motion (Figure 18a) toward NE for the relative displacement between KASH station in the southern DFS block and SHIR station in the northern block (Figure 18b). The NE direction of the motion is perpendicular to the strike of the EFZ implying reverse/thrust faulting along the fault zone (Figure 18c). The acute angle (∼45°) between the strike of both the CFZ and WFZ and the overall GPS motion implies oblique-slip reverse left-lateral faulting along these fault zones (Figure 18). Interestingly, the predicted GPS-derived motions along both the EFZ and WFZ are consistent with the present-day kinematics of these fault zones deduced from our geomorphic and structural data (section 4.1). But, the predicted GPS-derived oblique-slip reverse left-lateral faulting along the CFZ is not compatible with the pure left-lateral faulting demonstrated in this study (sections 4 and 5.2) and by *Fattahi et al.* [2007]. In this geodynamic context, the question to know is how the CFZ remains pure strike-slip, while, the NE relative motion between the southern and northern fault blocks implies a component of vertical faulting along the fault zone (Figures 18a and 18c)?

[50] Actually, such a discrepancy is explained by the partitioning of overall slip along the CFZ and other adjacent parallel faults (Figure 18c). The northward component of the NE relative motion is partially transferred northward along the Dahan-Qaleh fault zone (section 4.1) and is taken up by reverse faults at the northern side of the CFZ such as the Sabzevar and Kuh Sorkh faults [e.g., *Fattahi et al.*, 2006; *Hollingsworth et al.*, 2010]. The Dahan-Qaleh fault zone divides the northern side of the DFS into two individual fault blocks and merges into the DFS (Figure 18). Left-lateral faulting along the Dahan-Qaleh fault zone implies a SW translation of its western block relative to the WFZ. Along the WFZ, this relative movement is resolved into reverse and left-lateral components of faulting, which the reverse component is predominant (Figure 18a). This mechanism clearly explains the drastic change in the geomorphology of the DFS, and the decreasing left-lateral offsets from the CFZ to the WFZ just west of the intersection point between the

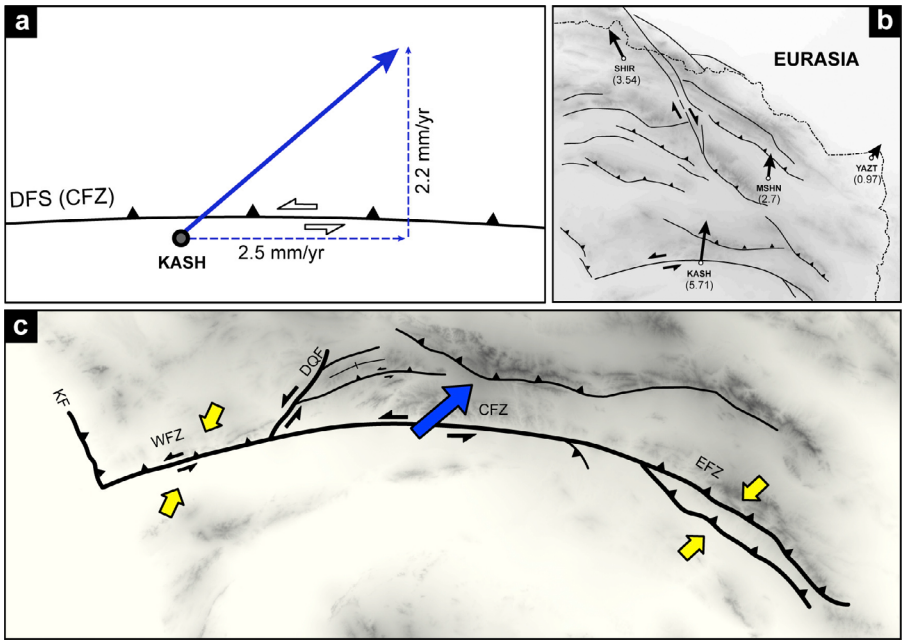

Figure 18. A simplified tectonic model to describe the present-day kinematics of the DFS based on the data and deduced results presented in this study. Blue arrow is the GPS-derived vector (3.3 mm/yr) of active motion between the southern and northern blocks of the DFS. This velocity vector (Figure 18a) was calculated from the relative motion between SHIR and KASH stations (Figure 18b) reported by *Masson et al.* [2007]. Yellow arrows illustrate the theoretical direction of the contraction suggested along the WFZ and EFZ. According to our geomorphic and structural data, there is no evidence of shortening across the CFZ suggesting that the contractional component of deformation is transferred northward, and is accommodated by geological reverse faulting and folding to the north of the CFZ. It is noteworthy that the 2.5 mm/yr presented in this model is an "assumed maximum" slip rate derived from differential GPS velocities between SHIR and KASH stations, which is different from and independent to the geomorphic-derived 2.5 mm/yr slip rate proposed by *Fattahi et al.* [2007].

Dahan-Qaleh fault zone and WFZ (section 4.1.1). The eastward component of the NE relative motion is assumed to be principally accommodated by left-lateral faulting along the DFS, which in turn, contributes to thrust faulting along the imbricate reverse faults at the EFZ restraining fault termination (Figure 18c).

[51] Interestingly, slip partitioning along the CFZ can explain the occurrence of the 14/12/1994 and 02/02/2000 earthquakes that indicate nearly pure thrust faulting on E-W fault planes parallel to the CFZ (section 3 and Figure 3).

[52] Preexisting tectonic models are principally based on fault block rotation theory [*Jackson and McKenzie*, 1984; *Walker et al.*, 2004; *Walker and Jackson*, 2004]. In all these models, the focus of discussions has been the curvature, rather than kinematics of the Doruneh Fault.

[53] The model proposed by *Walker and Jackson* [2004] assumes that eastward increasing slip rates on N-trending sets of right-lateral faults (e.g., Dehshir, Anar, Nayband and Nehbandan faults) could cause clockwise block rotation around vertical axes, which in turn, allows the Doruneh Fault to accommodate the northward motion of Central Iran relative to Eurasia. The maximum curvature in the trace of the Doruneh Fault has been related to the highest slip rate on the Sistan suture zone. However, key observations oppose some basics of this model.

[54] First, the definition of block rotation is unclear. Regardless the fact that block rotation models are based on the continuum deformation hypothesis, which requires specific conditions [e.g., *Thatcher*, 1995, 2003; *Shabanian et al.*, 2009b, and references therein], the first step to establish such a model is to define the geometry of individual rotating rigid blocks. In theory, the "planar" Doruneh Fault separates two distinct tectonic domains. The southern side comprises several block-like regions bounded by N-S right-lateral faults (Figure 1). The northern side (NE Iran) is a complex deformation domain affected by ~WNW-trending reverse/thrust faults together with other differently directed strike-slip faults [*Fattahi et al.*, 2006; *Hollingsworth et al.*, 2010; *Shabanian et al.*, 2009a, 2009b, 2010]. Neither the northern nor the southern sides of the Doruneh Fault can be considered as individual rigid blocks. Moreover, the non-uniform rotation of the Doruneh Fault [*Walker and Jackson*, 2004] requires that assumed rigid blocks at either side to be deformed. Indeed, if the fault bounded domains are deformable, the possible change in the orientation of the Doruneh Fault is only a simple structural deflection, not block rotation.

[55] Second, there is no evidence indicating that the 600-km-long Doruneh Fault, with an unknown geological history, was initially an E-trending straight fault [*Walker and Jackson*, 2004]. In addition, the suggestion of an initial E-W Doruneh Fault is already discarded by the present-day orientation of the fault; the eastern and western parts of

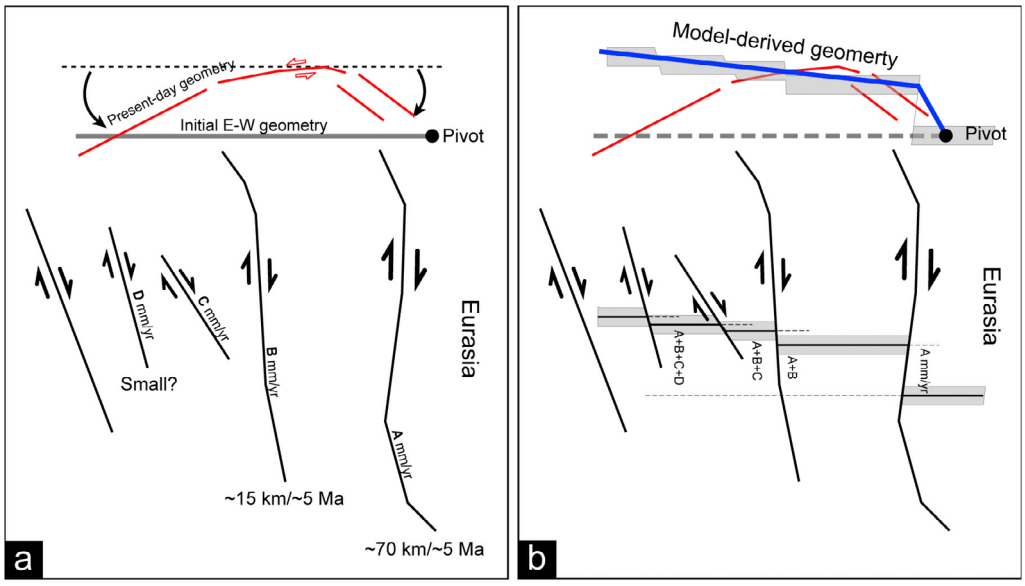

Figure 19. Simplified tectonic model to examine the hypothesis of clockwise block rotation proposed by *Walker and Jackson* [2004]. The main faults of central and eastern Iran are shown in Figure 19a. Thick gray line indicates the hypothetical E-W geometry of the DFS suggested by *Walker and Jackson* [2004]. To achieve the present-day geometry of the DFS the fault trace needs to rotate clockwise in the eastern part and counterclockwise in the western part. (b) The model-derived geometry of the DFS caused by eastward increasing slip rates along the N-S right-lateral faults.

the Doruneh Fault imply rotations in opposite directions with respect to an assumed initial E-W line (Figure 19a).

[56] The more fundamental issue is that individual fault slip rates, which have been used to explain the eastward increasing clockwise rotation of the Doruneh Fault [*Walker and Jackson*, 2004], cannot be directly integrated in the geodynamic context. But, those to be converted to relative displacements with respect to Eurasia. More precisely, despite the eastward increasing slip rates of two adjacent fault-bounded blocks, the northward motion of the fault-bounded blocks relative to Eurasia increase westward as slip rates of other western faults are added (Figure 19b). In such a way, the westernmost block (central Iran) moves faster than all eastern blocks implying the highest shear rate and largest northward displacement for the westernmost block with respect to Eurasia [e.g., *Reilinger et al.*, 2006]. As a result, the initial E-W Doruneh Fault assumed by *Walker and Jackson* [2004] would changes into a final NW-striking fault, incompatible with the present-day geometry of the Doruneh Fault (Figure 19b).

[57] As it is explained above, neither eastward increasing fault slip rates nor westward increasing shear rates relative to Eurasia can explain the present-day geometry of the Doruneh Fault. Aside from all these discrepancies, it is difficult to explain different kinematics of the WFZ, CFZ, and EFZ by a clockwise rotation of the Doruneh Fault.

6.2. Initiation of Strike-Slip Faulting Along the Doruneh Fault System

[58] Along the DFS, the maximum left-lateral offset (840 $\pm$ 70 m) is recorded by a Quaternary alluvial fan surface (Q3). But, the total cumulative displacement of the fault is unknown. Nevertheless, various crosscutting relationships between faults and other geological structures within the fault system allowed us to estimate a possible onset age for the present-day strike-slip faulting along the DFS.

[59] As discussed in section 3, early post Eocene vertical movements (normal or reverse faulting) of the DFS had continued to the Miocene time causing the subsidence of the southern Neogene sedimentary basin with respect to the northern pre-Oligocene paleoreliefs. Subsequently, Miocene marls and sandstones together with Pliocene conglomerates have been folded and faulted at the eastern termination of the DFS. These contractional structures are likely due to the compressional tectonic regime which, along the EFZ, is partly resulted from left-lateral strike-slip faulting along the CFZ (section 6.1). Such a suggestion implies that left-lateral strike slip faulting along the DFS may have started after Miocene or during Pliocene.

[60] On the other hand, the knife-cut trace of the Great Kavir Fault runs through the Dasht-e Kavir depression, and left-laterally displaced the post Miocene dome and basin structures (Figure 2b). This crosscutting relationship indicates a maximum Pliocene age ($\leq$5 Ma) for the initiation of strike slip faulting along the Great Kavir Fault. These age estimates are rather consistent with the post-Miocene ($\sim$4 Ma) tectonic reorganization that caused regional strike-slip faulting in NE Iran [*Shabanian et al.*, 2009a, 2009b].

7. Conclusion

[61] The structural and geomorphic investigations presented in this paper revealed that the curved shape DFS is a structural assemblage of three distinct fault zones, i.e., WFZ, CFZ, and EFZ; instead of, a 400-km-long uniform structure. Each fault zone is characterized by its own geometry and kinematics leading to discrete structural and geomorphic

characteristics. It seems, thus, unlikely that the "Doruneh Fault," including the Great Kavir Fault, could rupture along the entire ~600 km length to produce earthquakes of $M \geq 8$.

[62] The onset of strike-slip faulting along both the DFS and Great Kavir Fault is suggested at ≤5 Ma that is probably concurrent with the major tectonic reorganization reported in NE Iran [*Shabanian et al.*, 2009a, 2009b].

[63] In the kinematic model presented in this study (Figure 18c), the overall northeastward motion between central Iran - Lut and NE Iran is taken up by reverse left-lateral oblique-slip faulting along the WFZ and reverse faulting along the EFZ. In the central part, partitioning of slip into strike-slip and reverse component of faulting on parallel faults allows the CFZ to remain pure left-lateral strike-slip, while the overall convergence vector and slip on the fault are perpendicular. Such a model helps to better understand the geodynamic role of the DFS in the accommodation of ongoing Arabia-Eurasia convergence. Our data and the deduced results indicate that even continuous large strike-slip faults may be divided into several discrete fault zones to take up more easily overall tectonic motions. Such a deformation pattern may has further implications in other tectonic domains affected by perpendicular sets of strike-slip faults that accommodate crustal shortening in ways that the relationship between the overall convergence vector and slip on faults is drastically different.

[64] **Acknowledgments.** This work was funded by the INSU-CNRS (France) and partly by the International Institute of Earthquake Engineering and Seismology (IIEES, Iran), supervised by D. Hatzfeld, M. Ghafouri Ashtiani, and A. A. Tasnimi. We thank M. Zare (IIEES) for support and administrative assistance. Funding was provided by the Dyeti and PNRN programs (INSU-CNRS) and ACI FNS program (French Ministry of Research), within the above-mentioned cooperative agreement. SPOT images were provided thanks to the ISIS projects 4, 76, and 77 (©CNES 2007 to 2008, distribution SPOT images S.A.). Y. Farbod benefits of a Foreign Affair Ministry (Ministère des Affaires Etrangères, France) grant through the French Embassy in Iran. We thank V. Grimault, Ch. Duhamel, and the staff of the SCAC of the French Embassy in Tehran for their support. We are grateful to R. T. Walker, K. Hessami Azar, an anonymous reviewer, and an Associate Editor for helpful and constructive reviews. The Editor, Onno Oncken, is acknowledged for help and handling the manuscript. The general government of Khorassan-e Jonubi (Southern Khorassan) province has efficiently helped us during two field works in 2007 and 2010.

References

Adams, J., P. W. Basham, and S. Halchuk (1995), Northeastern North American earthquake potential: New challenges for seismic hazard mapping, *Curr. Res. Geol. Surv. Can.*, *1995-D*, 91–99.

Alavi-Naini, M., M. J. Vaezi-Pour, N. Alavi Tehrani, A. Behrouzi, and M. H. Kholghi (1992), Torbat-e Heidariyeh, in *Geological Map of Iran*, sheet K-5, scale 1:250,000, Geol. Surv. of Iran, Tehran.

Allen, M. B., R. Walker, J. A. Jackson, E. J. P. Blanc, M. Talebian, and M. Ghassemi (2006), Contrasting styles of convergence in the Arabia-Eurasia collision: Why escape tectonics does not occur in Iran, *Spec. Pap. Geol. Soc. Am.*, *409*, 579–589.

Ambraseys, N., and C. Melville (1982), *A History of Persian Earthquakes*, Cambridge Univ. Press, Cambridge, U. K.

Barka, A. A., and K. Kadinsky-Cade (1988), Strike-slip fault geometry in Turkey and its influence on earthquake activity, *Tectonics*, *7*, 663–684, doi:10.1029/TC007i003p00663.

Barka, A., et al. (2002), The surface rupture and slip distribution of the 17 August 1999 Izmit earthquake, (M 7.4), North Anatolian fault, *Bull. Seismol. Soc. Am.*, *92*(1), 43–60, doi:10.1785/0120000841.

Bellier, O., and M. L. Zoback (1995), Recent state of stress change in the Walker Lane zone, western Basin and Range Province, United States, *Tectonics*, *14*(3), 564–593, doi:10.1029/94TC00596.

Berberian, M., and R. Yeats (1999), Patterns of Historical Earthquake rupture in the Iranian Plateau, *Bull. Seismol. Soc. Am.*, *89*, 120–139.

Berberian, M., and R. Yeats (2001), Contribution of archaeological data to studies of earthquake history in the Iranian Plateau, *J. Struct. Geol.*, *23*, 563–584, doi:10.1016/S0191-8141(00)00115-2.

Bruhn, R. L., P. R. Sibler, and W. T. Parry (1987), Rupture characteristics of normal faults: An example from the Wasatch fault zone, Utah, in *Continental Extensional Tectonics*, edited by M. P. Coward, J. F. Dewey, and P. L. Hancock, *Geol. Soc. Spec. Publ.*, *28*, 337–353.

Budding, E., D. Schwartz, and D. Oppenheim (1991), Slip rate, earthquake recurrence, and seismogenic potential of the Rodgers Creek Fault Zone, northern California: Initial results, *Geophys. Res. Lett.*, *18*(3), 447–450, doi:10.1029/91GL00465.

Carey, E. (1979), Recherche des directions principales de contraintes associées au jeu d'une population de failles, *Rev. Geol. Dyn. Geogr. Phys.*, *21*, 57–66.

Carey, E., and B. Brunier (1974), Analyse théorique et numérique d'un modèle mécanique élémentaire appliqué à l'étude d'une population de failles, *C. R. Seances Acad. Sci., Ser. D*, *179*, 891–894.

Coppersmith, K. J. (1988), Temporal and spatial clustering of earthquake activity in the central and eastern United States, *Seismol. Res. Lett.*, *59*, 299–304.

DePolo, C. M., D. G. Clark, D. B. Slemmons, and A. Ramallie (1991), Historical basin and range province surface faulting and fault segmentation, *J. Struct. Geol.*, *13*, 123–136, doi:10.1016/0191-8141(91)90061-M.

Eftekhar-Nezhad, J., A. Aghanabati, B. Hamzehpour, and V. Baroyant (1976), Kashmar, in *Geological Map of Iran*, sheet J5, scale 1: 250,000, Geol. Surv. of Iran, Tehran.

Fattahi, M., R. Walker, J. Hollingsworth, A. Bahroudi, H. Nazari, M. Talebian, S. Armitage, and S. Stokes (2006), Holocene slip-rate on the Sabzevar thrust fault, NE Iran, determined using optically stimulated luminescence (OSL), *Earth Planet. Sci. Lett.*, *245*, 673–684, doi:10.1016/j.epsl.2006.03.027.

Fattahi, M., R. T. Walker, M. M. Khatib, A. Dolati, and A. Bahroudi (2007), Slip-rate estimate and past earthquakes on the Doruneh fault, eastern Iran, *Geophys. J. Int.*, *168*, 691–709, doi:10.1111/j.1365-246X.2006.03248.x.

Giessner, K., H. Hagedorn, and M. Sarvati (1984), Geomorphological studies in the Kashmar region (NE Iran), *Neues Jahrb. Geol. Palaeontol. Abh.*, *168*, 545–557.

Hessami, K., F. Jamali, and H. Tabassi (2003), Major active faults of Iran, scale 1:2,500,000, Int. Inst. of Earthquake Eng. and Seismol., Tehran.

Hollingsworth, J., J. Jackson, R. Walker, M. Gheitanchi, and M. Bolourchi (2006), Strike-slip faulting, rotation, and along-strike elongation in the Kopeh Dagh mountains, NE Iran, *Geophys. J. Int.*, *166*, 1161–1177, doi:10.1111/j.1365-246X.2006.02983.x.

Hollingsworth, J., M. Fattahi, R. Walker, M. Talebian, A. Bahroudi, M. J. Bolourchi, J. Jackson, and A. Copley (2010), Oroclinal bending, distributed thrust and strike-slip faulting, and the accommodation of Arabia–Eurasia convergence in NE Iran since the Oligocene, *Geophys. J. Int.*, *181*, 1214–1246, doi:10.1111/j.1365-246X.2010.04591.x.

Huber, H. (1977), North Central Iran and North East Iran, in *Geological Map of Iran*, sheets 2 and 3, scale 1:1,000,000, Natl. Iranian Oil Co., Tehran.

Ikeda, M., S. Toda, S. Kobayashi, Y. Ohno, N. Nishizaka, and I. Ohno (2009), Tectonic model and fault segmentation of the Median Tectonic Line active fault system on Shikoku, Japan, *Tectonics*, *28*, TC5006, doi:10.1029/2008TC002349.

Jackson, J., and D. McKenzie (1984), Active tectonics of the Alpine-Himalayan Belt between Turkey and Pakistan, *Geophys. J. R. Astron. Soc.*, *77*(1), 214–245.

Javidfakhr, B., O. Bellier, E. Shabanian, S. Ahmadian, and A. Saidi (2011), Plio-Quaternary tectonic regime changes in the transition zone between Alborz and Kopeh Dagh mountain ranges (NE Iran), *Tectonophysics*, *506*(1–4), 86–108, doi:10.1016/j.tecto.2011.04.013.

Keller, E. A., D. B. Seaver, D. L. Laduzinsky, D. L. Johnson, and T. L. Ku (2000), Tectonic geomorphology of active folding over buried reverse faults: San Emigdio Mountain front, southern San Joaquin Valley, California, *Geol. Soc. Am. Bull.*, *112*(1), 86–97, doi:10.1130/0016-7606(2000)112<86:TGOAFO>2.0.CO;2.

King, G. C. P., and J. Nabelek (1985), Role of fault bends in the initiation and termination of earthquake rupture, *Science*, *228*, 984–987, doi:10.1126/science.228.4702.984.

Knuepfer, P. L. K. (1989), Implication of the characteristics of end-points of historical surface fault ruptures for the nature of fault segmentation, *U.S. Geol. Surv. Open File Rep.*, *89–315*, 193–228.

Kondo, H., Y. Awata, O. Emre, A. Dougan, S. Ozalp, F. Tokay, C. Yildirim, T. Yoshioka, and K. Okumura (2005), Slip distribution, fault geometry, and fault segmentation of the 1944 Bolu-Gerede earthquake rupture,

North Anatolian fault, Turkey, *Bull. Seismol. Soc. Am.*, *95*, 1234–1249, doi:10.1785/0120040194.

Lees, J. M., and C. Nicholson (1993), Three-dimensional tomography of the 1992 southern California earthquake sequence: Constraints on dynamic earthquake rupture, *Geology*, *21*, 387–390, doi:10.1130/0091-7613(1993)021<0387:TDTOTS>2.3.CO;2.

Lettis, W., J. Bachhuber, R. Witter, C. Brankman, C. E. Randolph, A. Barka, W. D. Page, and A. Kaya (2002), Influence of releasing step-overs on surface fault rupture and fault segmentation: Examples from the 17 August 1999 izmit earthquake of the North Anatolian Fault, Turkey, *Bull. Seismol. Soc. Am.*, *92*(1), 19–42, doi:10.1785/0120000808.

Masson, F., J. Chery, D. Hatzfeld, J. Marttinod, P. Vernant, F. Tavakoli, and M. Ghafory-Ashtiani (2005), Seismic versus aseismic deformation in Iran inferred from earthquake and geodetic data, *Geophys. J. Int.*, *160*, 217–226, doi:10.1111/j.1365-246X.2004.02465.x.

Masson, F., M. Anvari, Y. Djamour, A. Walpersdorf, F. Tavakoli, M. Daignieres, H. Nankali, and S. Van Gorp (2007), Large-scale velocity field and strain tensor in Iran inferred from GPS measurements: New insight for the present-day deformation pattern within NE Iran, *Geophys. J. Int.*, *170*, 436–440, doi:10.1111/j.1365-246X.2007.03477.x.

McCalpin, J. P. (Ed.) (1996), *Paleoseismology*, Academic, San Diego, Calif.

McClusky, S., R. Reilinger, S. Mahmoud, D. Ben Sari, and A. Tealeb (2003), GPS constraints on Africa (Nubia) and Arabia plate motions, *Geophys. J. Int.*, *155*(1), 126–138, doi:10.1046/j.1365-246X.2003.02023.x.

Meyer, B., and K. Le Dortz (2007), Strike-slip kinematics in Central and eastern Iran: Estimating fault slip rates averaged over the Holocene, *Tectonics*, *26*, TC5009, doi:10.1029/2006TC002073.

Mohajer-Ashjai, A. (1975), Recent and contemporary crustal deformation in eastern Iran, Ph.D. thesis, Imperial College, London.

Nazari, H., M. Fattahi, B. Meyer, M. Sebrier, M. Talebian, M. Foroutan, K. Le Dortz, M. D. Bateman, and M. Ghorashi (2009), First evidence for large earthquakes on the Deshir Fault, Central Iran Plateau, *Terra Nova*, *21*, 417–426, doi:10.1111/j.1365-3121.2009.00892.x.

Nishigami, K. (2000), Deep crustal heterogeneity along and around the San Andreas fault system in central California and its relation to the segmentation, *J. Geophys. Res.*, *105*, 7983–7998, doi:10.1029/1999JB900381.

Regard, V., O. Bellier, J.-C. Thomas, M. R. Abbassi, J. Mercier, E. Shabanian, K. Feghhi, and S. Soleymani (2004), Accommodation of Arabia-Eurasia convergence in the Zagros-Makran transfer zone, SE Iran: A transition between collision and subduction through a young deforming system, *Tectonics*, *23*, TC4007, doi:10.1029/2003TC001599.

Regard, V., et al. (2005), Cumulative right-lateral fault slip rate across the Zagros–Makran transfer zone: Role of the Minab–Zendan fault system in accommodating Arabia–Eurasia convergence in southeast Iran, *Geophys. J. Int.*, *162*, 177–203, doi:10.1111/j.1365-246X.2005.02558.x.

Reilinger, R., et al. (2006), GPS constraints on continental deformation in the Africa-Arabia-Eurasia continental collision zone and implications for the dynamics of plate interactions, *J. Geophys. Res.*, *111*, B05411, doi:10.1029/2005JB004051.

Ritz, J. F., H. Nazari, A. Ghassemi, R. Salamati, A. Shafei, S. Soleymani, and P. Vernant (2006), Active transtension inside central Alborz: A new insight into northern Iran–southern Caspian geodynamics, *Geology*, *34*, 477–480, doi:10.1130/G22319.1.

Schwartz, D. P., and K. J. Coppersmith (1984), Fault behavior and characteristic earthquakes' examples from the Wasatch and San Andreas fault zones, *J. Geophys. Res.*, *89*, 5681–5698, doi:10.1029/JB089iB07p05681.

Schwartz, D. P., and R. H. Sibson (Eds.) (1989), *Fault Segmentation and Controls of Rupture Initiation and Termination*, *U.S. Geol. Surv. Open File Rep.*, *89–315*, Menlo Park, Calif.

Sella, G. F., T. H. Dixon, and A. Mao (2002), REVEL: A model for Recent plate velocities from space geodesy, *J. Geophys. Res.*, *107*(B4), 2081, doi:10.1029/2000JB000033.

Shabanian, E., L. Siame, O. Bellier, L. Benedetti, and M. R. Abbassi (2009a), Quaternary slip rates along the northeastern boundary of the Arabia–Eurasia collision zone (Kopeh Dagh Mountains, Northeast Iran), *Geophys. J. Int.*, *178*, 1055–1077, doi:10.1111/j.1365-246X.2009.04183.x.

Shabanian, E., O. Bellier, L. Siame, N. Arnaud, M. R. Abbassi, and J.-J. Cochemé (2009b), New tectonic configuration in NE Iran: Active strike-slip faulting between the Kopeh Dagh and Binalud mountains, *Tectonics*, *28*, TC5002, doi:10.1029/2008TC002444.

Shabanian, E., O. Bellier, M. R. Abbassi, L. Siame, and Y. Farbod (2010), Plio-Quaternary stress states in NE Iran: Kopeh Dagh and Allah Dagh-Binalud mountain ranges, *Tectonophysics*, *480*, 280–304, doi:10.1016/j.tecto.2009.10.022.

Solaymani, A. S. (2009), Seismic hazard assessment for Tehran, Tabriz and Zanjan cities (NW Iran) based on morphotectonics and paleoseismology, Ph.D. thesis, 150 pp., Univ. of Montpellier, Montpellier, France.

Stewart, M. E., and W. J. Taylor (1996), Structural analysis and fault segment boundary identification along the Hurricane fault in southwestern Utah, *J. Struct. Geol.*, *18*(8), 1017–1029, doi:10.1016/0191-8141(96)00036-3.

Stocklin, J. and M. H. Nabavi (1973), Tectonic map of Iran, scale 1: 2,500,000, Geol. Surv. of Iran, Tehran.

Sylvester, A. (1988), Strike-slip faults, *Geol. Soc. Am. Bull.*, *100*, 1666–1703, doi:10.1130/0016-7606(1988)100<1666:SSF>2.3.CO;2.

Tavakoli, F. (2007), Present-day kinematics of the Zagros and east of Iran faults, Ph.D. thesis, Univ. of Joseph Fourier, Grenoble, France. [Available at http://tel.archives-ouvertes.fr/tel-00285919/fr/.]

Tchalenko, J. S. (1973), The Kashmar (Turshiz) 1903 and Torbat-e-Heidariyeh (south) earthquakes in Central Khorassan (Iran), *Ann. Geofis.*, *26*(1), 29–40.

Tchalenko, J. S., and M. Berberian (1975), Dasht-e-Bayez fault, Iran: Earthquake and earlier related structures in bedrock, *Geol. Soc. Am. Bull.*, *86*, 703–709.

Tchalenko, J. S., M. Berberian, and H. Behzadi (1973), Geomorphic and seismic evidence for recent activity on the Doruneh Fault, Iran, , *Tectonophysics*, *19*, 333–341, doi:10.1016/0040-1951(73)90027-9.

Thatcher, W. (1995), Microplate versus continuum descriptions of active tectonic deformation, *J. Geophys. Res.*, *100*, 3885–3894, doi:10.1029/94JB03064.

Thatcher, W. (2003), GPS constraints on the kinematics of continental deformation, *Int. Geol. Rev.*, *45*, 191–212, doi:10.2747/0020-6814.45.3.191.

Tirrul, R., I. R. Bell, R. J. Griffis, and V. E. Camp (1983), The Sistan suture zone of eastern Iran, *Geol. Soc. Am. Bull.*, *94*, 134–150, doi:10.1130/0016-7606(1983)94<134:TSSZOE>2.0.CO;2.

Vernant, P., et al. (2004), Present-day crustal deformation and plate kinematics in the Middle East constrained by GPS measurements in Iran and northern Oman, *Geophys. J. Int.*, *157*(1), 381–398, doi:10.1111/j.1365-246X.2004.02222.x.

Walker, R., and J. Jackson (2004), Active tectonics and late Cenozoic strain distribution in central and eastern Iran, *Tectonics*, *23*, TC5010, doi:10.1029/2003TC001529.

Walker, R., J. Jackson, and C. Baker (2003), Surface expression of thrust faulting in eastern Iran: Source parameters and surface deformation of the 1978 Tabas and 1968 Ferdows earthquake sequences, *Geophys. J. Int.*, *152*, 749–765, doi:10.1046/j.1365-246X.2003.01886.x.

Walker, R., J. Jackson, and C. Baker (2004), Active faulting and seismicity of the Dasht-e-Bayaz region, eastern Iran, *Geophys. J. Int.*, *157*, 265–282, doi:10.1111/j.1365-2966.2004.02179.x.

Walker, R. T., and M. Fattahi (2011), A framework of Holocene and Late Pleistocene environmental change in eastern Iran inferred from the dating of periods of alluvial fan abandonment, river terracing, and lake deposition, *Quat. Sci. Rev.*, *30*, 1256–1271, doi:10.1016/j.quascirev.2011.03.004.

Wallace, R. E. (1970), Earthquake recurrence intervals on the San Andreas Fault, *Geol. Soc. Am. Bull.*, *81*, 2875–2890, doi:10.1130/0016-7606(1970)81[2875:ERIOTS]2.0.CO;2.

Wellman, H. W. (1966), Active wrench faults of Iran Afghanistan and Pakistan, *Geol. Rundsch.*, *55*, 716–735.

Wells, D. L., and K. J. Coppersmith (1994), New empirical relationships among magnitude, rupture length, rupture width, rupture area, and surface displacement, *Bull. Seismol. Soc. Am.*, *84*(4), 974–1002.

Woodcock, N. H., and M. Fischer (1986), Strike-slip duplexes, *J. Struct. Geol.*, *8*, 725–735, doi:10.1016/0191-8141(86)90021-0.

Wulff, H. E. (1968), The Qanats of Iran, *Sci. Am.*, *218*, 94–105, doi:10.1038/scientificamerican0468-94.

M. R. Abbassi, International Institute of Earthquake Engineering and Seismology, Tehran, Iran. (mrabbassi2000@yahoo.com)

O. Bellier, Y. Farbod, and E. Shabanian, Aix-Marseille Université, CEREGE, UMR 6635, BP 80, Europôle de l'Arbois, F-13545 Aix en Provence CEDEX 4, France. (bellier@cerege.fr; farbod@cerege.fr; shabanian@cerege.fr)